J. Fluid Mech. (1992), *vol.* 238, *pp.* 119–154
Printed in Great Britain

Heat-transfer enhancement due to slender recirculation and chaotic transport between counter-rotating eccentric cylinders

By S. GHOSH[1], H.-C. CHANG[1]† AND M. SEN[2]

[1] Department of Chemical Engineering, University of Notre Dame, Notre Dame, IN 46556, USA

[2] Department of Aerospace and Mechanical Engineering, University of Notre Dame, Notre Dame, IN 46556, USA

(Received 1 July 1991)

Using Stokes flow between eccentric, counter-rotating cylinders as a prototype for bounded, nearly parallel lubrication flow, we investigate the effect of a slender recirculation region within the flow field on cross-stream heat or mass transport in the important limit of high Péclet number Pe where the enhancement over pure conduction heat transfer without recirculation is most pronounced. The steady enhancement is estimated with a matched asymptotic expansion to resolve the diffusive boundary layers at the separatrices which bound the recirculation region. The enhancement over pure conduction is shown to vary as $\epsilon^{\frac{1}{2}}$ at infinite Pe, where $\epsilon^{\frac{1}{2}}$ is the characteristic width of the recirculation region. The enhancement decays from this asymptote as $Pe^{-\frac{1}{3}}$. If one perturbs the steady flow by a time-periodic forcing, fast relative to the convective and diffusive times, the separatrices undergo a homoclinic entanglement which allows fluid elements to cross the separatrices. We establish the existence of this homoclinic entanglement and show that the resulting chaotic particle transport further enhances the cross-stream flux. We estimate the penetration of the fluid elements across the separatrices and their effective diffusivity due to this chaotic transport by a Melnikov analysis for small-amplitude forcing. These and the steady results then provide quantitative estimates of the time-averaged transport enhancement and allow optimization with respect to system parameters. An optimum forcing frequency which induces maximum heat-transfer enhancement is predicted and numerically verified. The predicted optimum frequency remains valid at strong forcing and large Pe where chaotic transport is as important as the recirculation mechanism. Since most heat and mass transport devices operate at high Pe, our analysis suggests that chaotic enhancement can improve their performance and that a small amplitude theory can be used to optimize its application.

1. Introduction

In many engineering applications, the pertinent heat or mass transport is across a unidirectional flow field. Even at high flow rates, such cross-stream transport is essentially dominated by diffusion/conduction and is extremely inefficient. (We shall focus on heat transport subsequently but the thermal diffusivity will be referred to as diffusivity for simplicity. The analogy to mass transport is obvious.) However, when the parallel flow is slightly disturbed such that a slender recirculation bubble

† Author to whom correspondence should be addressed.

appears within the flow, some convective flow is generated in the normal direction. As a result, significant increase in the cross-stream transport is observed even though the flow field is only slightly perturbed from parallel flow. For example, mass transport across a laminar falling film increases by as much as a factor of 10 when waves appear at the interface (Goren & Mani 1968). Although the waves introduce about a 10% increase in the interfacial area and the flow field beneath the waves remains nearly parallel, the chief mechanism behind the enhancement is the slender recirculation below the interface created by the waves. Similarly, heat transfer in helicoidal tubes (Chávez, Zhixue & Sen 1988), in grooved channels (Ghaddar *et al.* 1986) and in a heat exchanger tube with transverse vortices driven by the corona effect (Ohadi, Sharaf & Nelson 1991) have all been shown to increase significantly (orders of magnitude) when recirculations exist in the flow. We study this enhancement in cross-stream heat transfer with a prototype system of two-dimensional flow between counter-rotating eccentric cylinders (Aref & Balachandar 1986; Chaiken *et al.* 1986; Ottino 1989). The effects of bubble size and Péclet number are scrutinized. We shall also analyse the effect of perturbing the recirculation bubble with a fast time-periodic modulation. In this system, this is effected by periodically varying the rotation speed of the outer cylinder about a mean speed. Time-dependent disturbances, however, can also be introduced by intrinsic instabilities such as the travelling wave instabilities of the falling film and oscillatory Rayleigh–Bénard convection (Holmes 1984; Broomhead & Ryrie 1988; Solomon & Gollub 1988; Weiss & Knobloch 1989). The time-periodic perturbation actually introduces a second mechanism for transport enhancement. As discussed by Eckhardt (1990), the periodic forcing breaks up the bounding streamlines of the recirculation region, which are either homoclinic or heteroclinic orbits connecting stagnation points, and allows exchange of fluids with the outside region. A stroboscopic map of a particle affected by the time-periodic flow field of the present system reveals chaotic particle paths near the boundary of the recirculation region (Aref & Balachandar 1986; Chaiken *et al.* 1986; Ottino 1989; Swanson & Ottino 1990). In fact, this prototype is one of the first used to demonstrate the existence of Lagrangian chaos. We show that chaotic transport across a circulation boundary can be approximated by a diffusion process. We shall carry out a Melnikov analysis of the prototype system to estimate its enhanced transport rate due to this chaotic mixing. While earlier work has demonstrated both numerically and experimentally that chaotic particle paths can appear in the present system, our Melnikov analysis rigorously establishes their existence. More importantly, while others have speculated that the chaotic paths can enhance transport of heat and mass, the present Melnikov analysis actually offers a quantitative estimate of the enhancement. The contribution of chaotic transport is then properly added to molecular diffusion and advection-enhanced transport owing to the slender recirculation. An enhanced diffusion coefficient D_{eff} is introduced to quantitatively represent the transport flux enhancement due to these combined mechanisms. Our analysis provides an analytical estimate of D_{eff} as a function of system parameters and operating conditions. This estimate is favourably compared to numerical calculations and is hence used to optimize system design and operating conditions. At the optimal forcing frequency, for example, 100% enhancement over pure diffusion can be readily achieved.

There is a significant practical advantage in using Lagrangian chaos to enhance transport rate. Since Lagrangian chaos can be achieved at low, even creeping, flow conditions, the enhanced scalar transport is not associated with enhanced momentum transfer. This is in contrast to scalar transport enhancement by turbulent flow fields,

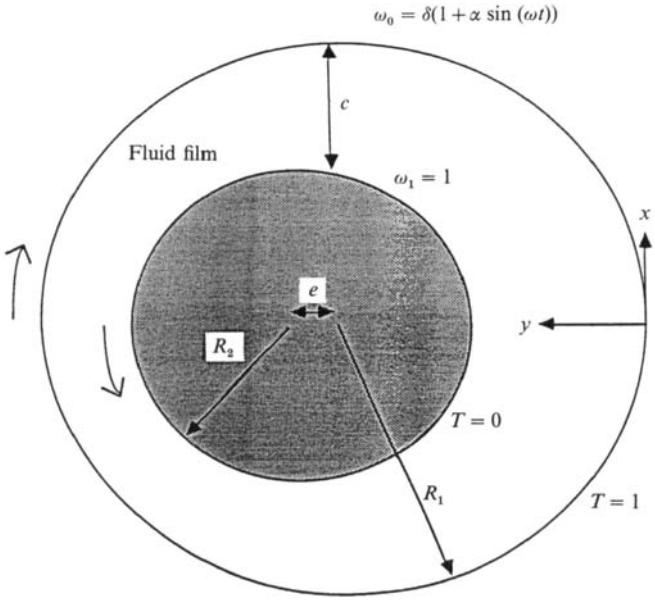

FIGURE 1. Schematic of the eccentric cylinder prototype. The local Cartesian coordinate is on the outer cylinder pointing inwards. The isothermal conditions are properly normalized and reduced such that it is unity at the outer wall ($y = 0$) and zero at the inner wall. The directions of the steady rotation of both cylinders are indicated. The parameters e and c are the eccentricity and clearance respectively.

which is usually at the expense of significant pressure drop and power expenditure. Low-Reynolds-number flow conditions also allow the luxury of numerical and even analytical optimization of system geometry and operating conditions to maximize enhancement. Recently, we have exploited these enhancement advantages of Lagrangian chaos to design an alternating-axis coiled heat-exchanger tube which enhances heat transfer by 10% with only a 3% increment in pressure drop over the conventional helical coil (Acharya, Sen & Chang 1992). (See also Saxena & Nigam, 1984, who speculated that this design can enhance heat transfer without any knowledge of Lagrangian chaos!)

The prototype eccentric cylinders are shown in figure 1 with the pertinent geometric parameters. When the two cylinders are rotated steadily in opposite directions, a slender recirculation region appears and is bounded by a separatrix Γ which connects to a hyperbolic stagnation point A and is a double homoclinic loop. The outer separatrix is denoted Γ_+ and the inner one Γ_-. These features of the flow field are clearly demonstrated in the numerically obtained pathlines in figure 2, where the gap width has been stretched by an arbitrary scale factor for clarity. Except for tracer particles on Γ and on the walls, particle trajectories convected by the steady flow field either traverse around the inner cylinder in regions Ω_1 and Ω_2 outside Γ or around the elliptic stagnation point B in region Ω_1 within the double homoclinic loop Γ. We shall impose isothermal boundary conditions on the outer and inner cylinders and estimate the overall heat transfer across the gap. A lubrication analysis in the limit of small gap width allows an estimate of the flow field within the gap. The trajectories in Ω_1 and Ω_2 are almost parallel to the two walls and the temperature on each streamline varies linearly away from the walls to leading order in the dimensionless eccentricity ϵ. Even at high rotation speeds, radial transport across the gap in Ω_1 and Ω_2 is still dominated by diffusion. The scenario is quite

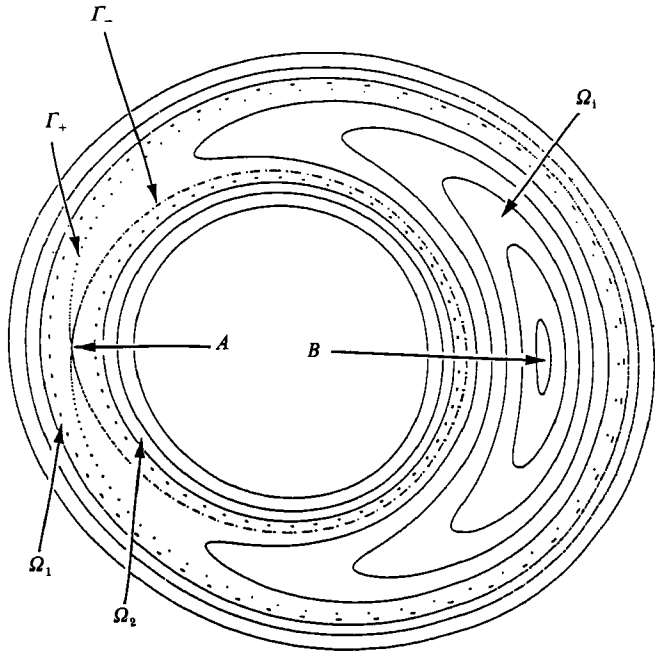

FIGURE 2. The steady streamlines within the gap. The recirculation region Ω_1 contains closed streamlines around the centre B. The separatrices Γ that bound Ω_1 are two homoclinic loops, Γ_+ on the outside and Γ_- on the inside. The segment of Γ_+ above A and the segment of Γ_- below A are the unstable manifolds of A while the other segments are the stable manifolds. The streamlines in the Ω_1 and Ω_2 regions outside Ω_1 are nearly parallel.

different within the circulation region, Ω_1. Here, streamlines close to Γ spend approximately equal time near Ω_1 and Ω_1 which have very different temperatures.

We have shown that the steady enhancement at low Péclet number Pe varies as $1+aPe^2$ (Ghosh 1991) where a is a constant depending on system geometry. This is identical to earlier results by Moffat (1983) and Sagues & Horsthemke (1986). Although chaotic transport still occurs at low Pe, it is negligible compared to thermal diffusion since it is induced by advection. We (Ghosh 1991) have shown that the time-averaged enhancement again varies as $1+aPe^2$. Since Pe is small, enhancement by either recirculation or chaotic transport is negligible at low Pe. This is dramatically different, however, at the high Pe limit when the steady cross-stream advection due to the recirculation and the chaotic transport due to time-periodic advection are far more important than diffusion. It should be noted that mass transfer devices necessarily operate at extremely high Pe and this is hence the far more important limit.

In the limit of high Péclet number, the circuit time of the circulation is much shorter than the diffusive timescale and mixing along each streamline effectively expels temperature gradients within this region at steady state. As a result, the recirculation region becomes a well-mixed region at steady state and this effectively reduces the radial distance for diffusive transport. Steady high-Péclet-number transport between recirculation cells has recently been examined by Shraiman (1987) and Rosenbluth *et al.* (1987). The same steady mixing mechanism is also present in these systems whose circulations are not slender. Hence, since the transport in their systems is between two well-mixed convective cells, the enhancement is determined

by a diffusive boundary layer of thickness $Pe^{-\frac{1}{2}}$ at the boundary of the two cells. (Their boundaries like ours are separatrices connecting stagnation points and the diffusive boundary layer is similar to those near mobile interfaces with a thickness that varies as $Pe^{-\frac{1}{2}}$; see review by Stewart 1977.) Consequently, the effective transport flux enhancement (or, effective diffusivity) across circulation cells varies as $Pe^{-\frac{1}{2}}$. Although a diffusive boundary layer also exists near Γ in the present problem, it lies only interior to Γ on the Ω_i side since the temperature fields within Ω_1 and Ω_2 are not well-mixed for our nearly parallel flow. As a result, the diffusive boundary layer contributes to second order in the transport enhancement and a constant asymptote exists at high Pe in our problem. This contrasts with the large degree of enhancement at high Pe for systems controlled by a diffusive boundary layer.

The above enhancement by a steady flow field exists only if the cylinders are eccentric. The recirculation region responsible for the enhancement does not appear when the cylinders are concentric. Similarly, stochastic particle trajectories induced by a time-periodic flow field also appear only if the cylinders are eccentric with respect to each other. This is because the time-periodic flow field is introduced by adding a small time-periodic component to the rotation speed of the outer cylinder. For concentric cylinders, the particles would simply oscillate periodically along each circular streamline without inducing any normal mixing between streamlines. We shall extract this important effect of eccentricity on the enhancement by carrying out an expansion for small eccentricity. With eccentric cylinders, a family of closed streamlines appear in Ω_i bounded by the homoclinic separatrix Γ in the steady case. In earlier simulations of related two-dimensional time-periodic flow fields (Broomhead & Ryrie 1988; Solomon & Gollub 1988; Weiss & Knobloch 1989; Rom-Kedar, Leonard & Wiggins 1990; Cox *et al.* 1990) it was shown that time-periodic modulation or disturbances produce stochastic layers both within Ω_i and near Γ, though the stochasticity is typically most pronounced in the vicinity of Γ. Since the region within Ω_i has already been thoroughly mixed by the steady flow field in the more interesting high-Péclet-number limit, the contribution to the time-averaged transport enhancement of the stochastic layers internal to Γ is negligible at large time. It is the invasion of the stochastic layer around Γ into the Ω_1 and Ω_2 regions, owing to entanglement of the stable and unstable manifolds of the hyperbolic stagnation point, that allows the time-periodic flow field to enhance heat transfer in our system. Thus, in the context of enhancement due to the chaotic motions, the separatrix layer is the most important once since it mixes fluid from outside the recirculation region with that within it. We shall estimate the width of the separatrix stochastic layer external to Γ, which is also the layer that invades into Ω_1 and Ω_2 and we shall refer it as the stochastic layer without any fear of ambiguity. We shall also estimate the diffusivity within the stochastic layer arising out of the chaotic particle motion, which Chirikov (1979) has shown to be a diffusion process at an appropriate limit. This, in conjunction with estimates of the width of the stochastic layer, allows analytical estimates of the overall time-averaged enhancement in the unsteady flow at the pertinent limit of high Pe. As mentioned earlier, this is the extremely important limit of industrial concern.

In §2, we carry out a lubrication analysis to obtain the time-dependent flow field in the limit of vanishing Reynolds number and small gap. The effect diffusivity for the steady flow field at high Péclet number is estimated in §3, which involves a resolution of the diffusive boundary layer on the inside of Γ. In §4 we estimate the width of the stochastic layer for small amplitudes of the periodic perturbation by using the Melnikov function to construct a separatrix map (Chirikov 1979; Weiss &

Knobloch 1989) which further reduces to the well-known standard map. We also show the existence of an optimum forcing frequency at which the stochastic layer is of maximum width and the stochasticity in most pronounced. Using these same techniques we show that the chaotic particle motion has all the characteristics of a Markov diffusion process in the radial direction with zero drift and finite diffusion coefficient, which we obtain in the appropriate limit of the system parameters. Finally, the time-averaged transport enhancement at large time for the perturbed system is estimated at the high Pe limit. All estimates are satisfactorily compared to numerical results from direct computation of the energy equation. It is also shown numerically in §4 that some of our analytical results for small time-periodic perturbations, such as the existence of an optimum forcing frequency, remain valid at large perturbations. The results are summarized in §5.

2. Lubrication analysis of flow in the gap

We shall derive the leading-order flow field within the gap in the limit of small c/R where c is the radial clearance and R is the radius of the inner cylinder which is also equal to the outer radius to leading order (see figure 1). The small clearance limit allows a simple lubrication derivation of the flow field in closed form. A more complicated flow field for arbitrary clearance but vanishingly small Reynolds number has been derived by Ballal & Rivlin (1976). Choosing a local Cartesian coordinate fixed on the wall of the outer cylinder as shown in figure 1, we scale the azimuthal coordinate by R and the radial coordinate by c. The azimuthal velocity is scaled by $R\omega_i$ where ω_i is the clockwise angular velocity of the inner cylinder and the radial velocity by $c\omega_i$. The dimensionless gap width is scaled by c, pressure by $\mu\omega_i(R/c)^2$ and time by $1/\omega_i$. In terms of the scaled variables, two independent parameters appear in the equations of motion, the Reynolds number $Re = c^2\omega_i/\nu$ and the dimensionless clearance $\lambda = c/R \ll 1$. Here μ is the viscosity and ν the kinematic viscosity of the fluid. We shall assume Re is of $O(\lambda)$ and to leading order in λ, namely, $O(\lambda^0)$ it does not enter the analysis. For the perturbed flow, we shall require the modulation frequency to be in excess of ω_i, $\omega \gg 1$, to allow a multi-time scale expansion. For the lubrication approximation to remain valid, we must then have the clearance to be small such that $c^2\omega/\nu$ remains of $O(\lambda^0)$. Under these conditions, the equations of motion and the pertinent boundary conditions are

$$\frac{\partial^2 u}{\partial y^2} = \frac{\partial p}{\partial x}, \tag{2.1}$$

$$\frac{\partial u}{\partial x} + \frac{\partial v}{\partial y} = 0, \tag{2.2}$$

$$\frac{\partial p}{\partial y} = 0, \tag{2.3}$$

$$u(y = 0) = -\delta(1 + \alpha \sin wt), \tag{2.4}$$

$$u(y = h) = 1, \tag{2.5}$$

$$v(y = 0) = 0, \tag{2.6}$$

$$v(y = h) = \frac{\mathrm{d}h}{\mathrm{d}x}, \tag{2.7}$$

$$p(x = 0) = p(x = 2\pi) = 0, \tag{2.8}$$

where x is the scaled azimuthal coordinate of the local Cartesian coordinate whose origin is at the widest portion of the gap, y is the scaled radial coordinate, and u and v are the dimensionless velocity components in the azimuthal and radial direction respectively. The parameter δ is the ratio of the steady outer rotating speed to the inner rotating speed. It is a positive parameter and the rotation is clockwise at the outer cylinder. The parameter α is the amplitude of the periodic perturbation and ω is the dimensionless forcing frequency scaled with respect to ω_1. Since both the pressure and flow fields are 2π periodic in x and the pressure field is defined up to an arbitrary constant, we choose (2.8) as a reference pressure. The dimensionless gap width $h(x)$ is, to leading order,

$$h = 1+\epsilon\cos x+O(\lambda). \tag{2.9}$$

The dimensionless eccentricity, $\epsilon = e/c$, is a small parameter less than unity where e is the eccentricity between the two cylinders. Thus ϵ is independent from the dimensionless clearance λ. We shall examine the case where ϵ is of a larger order than λ such that the analysis is up to $O(\lambda^0)$ and $O(\epsilon)$. In the subsequent analysis we shall carry out multiparameter expansions in several independent small parameters. Relative orders of these parameters must then be specified such that a consistent resolution is achieved. We shall, however, limit ourselves to zeroth order in λ. Consequently, the radius of the inner cylinder must be sufficiently large relative to the clearance such that λ is smaller than all other small parameters in our problem. In what follows, it will be understood that all expansions are valid to $O(\lambda^0)$ and specific mention of λ will be omitted for simplicity. In contrast, since the eccentricity ϵ is responsible for both the steady and the time-periodic enhancement, its expansion will be carefully carried out.

The lubrication equations, (2.1)–(2.9), are solved to these orders to obtain the flow field. It is convenient to express u and v as

$$\begin{aligned} u(x,y,t) &= \bar{u}(x,y)+\alpha\hat{u}(x,y)\sin\omega t \\ &= \bar{u}_0(y)+\epsilon\bar{u}_1(x,y)+\alpha[\hat{u}_0(y)+\epsilon\hat{u}_1(x,y)]\sin\omega t+O(\epsilon^2), \\ v(x,y,t) &= \epsilon\bar{v}_1(x,y)+\alpha[\epsilon\hat{v}_1(x,y)]\sin\omega t+O(\epsilon^2), \end{aligned}$$

where the time-independent and time-dependent components have been separated for clarity. These are given by

$$\bar{u}_0 = (1+\delta)\,y-\delta, \tag{2.10a}$$

$$\bar{u}_1 = 3(1-\delta)\,y^2\cos x+2(\delta-2)\,y\cos x, \tag{2.10b}$$

$$\hat{u}_0 = \delta(y-1), \tag{2.10c}$$

$$\hat{u}_1 = \delta(2y\cos x-3y^2\cos x), \tag{2.10d}$$

$$\bar{v}_1 = (1-\delta)\,y^3\sin x+(\delta-2)y^2\sin x, \tag{2.11a}$$

$$\hat{v}_1 = \delta[y^2(1-y)\sin x]. \tag{2.11b}$$

We note that u is of $O(\epsilon^0)$ while v is of $O(\epsilon^1)$ since the small radial flow in the slender recirculation bubble, which is chiefly responsible for both steady and perturbed enhancement, is created by eccentricity. Because inertia is negligible, the flow field reacts instantaneously to the perturbation at the outer cylinder. This time-periodic

two-dimensional flow field can be conveniently expressed in terms of a stream function

$$\psi(x,y,t) = \bar{\psi}(x,y) + \alpha\hat{\psi}(x,y,t), \tag{2.12}$$

where the steady component is expressed as

$$\bar{\psi}(x,y) = \bar{\psi}_0(y) + \epsilon\bar{\psi}_1(x,y) + O(\epsilon^2), \tag{2.13a}$$

with

$$\bar{\psi}_0(y) = \delta y - \tfrac{1}{2}(1+\delta)\,y^2, \tag{2.13b}$$

$$\bar{v}_1(x,y = (2-\delta)\,y^2\cos x - (1-\delta)\,y^3\cos x, \tag{2.13c}$$

and, similarly, the perturbation

$$\hat{\psi}(x,y,t) = \hat{\psi}_0(y) + \epsilon\hat{\psi}_1(x,y) + O(\epsilon^2), \tag{2.14a}$$

with

$$\hat{\psi}_0(y) = \delta[y(1-\tfrac{1}{2}y)]\sin\omega t, \tag{2.14b}$$

$$\hat{\psi}_1(x,y) = \delta[y^2(y-1)\cos x]\sin wt. \tag{2.14c}$$

The equations of motions are then formally that of a Hamiltonian system,

$$\dot{x} = -\frac{\partial\psi}{\partial y}(x,y,t), \tag{2.15}$$

$$\dot{y} = \frac{\partial\psi}{\partial x}(x,y,t), \tag{2.16}$$

and the stream function $\psi(x,y,t)$ is the Hamiltonian.

We shall further examine the steady flow field with $\alpha = 0$. For every azimuthal position x there is a radial location $y_*(x)$ in the flow where the steady azimuthal velocity $\bar{u}$ vanishes. At $x = 0$ and $x = \pi$ this point becomes a stagnation point as both $\bar{u}$ and $\bar{v}$ vanish at $y_*(x = 0)$ and $y_*(x = \pi)$. Thus, for small values of ϵ and all values of δ considered there are exactly two stagnation points in the flow field: a hyperbolic stagnation point, A, located at the narrowest part of the gap, given by $y_A = y_*(x = \pi)$, and an elliptic stagnation point, B, located at the widest part of the gap, given by $y_B = y_*(x = 0)$. The radial location of y_* at every x is given by

$$y_*(x) = \frac{\delta}{1+\delta} + \epsilon\frac{\delta(\delta^2-\delta+4)}{(1+\delta)^3}\cos x + O(\epsilon^2). \tag{2.17}$$

A is at $x = \pi$ with radial location

$$y_A = \frac{\delta}{1+\delta} - \epsilon\frac{\delta(\delta^2-\delta+4)}{(1+\delta)^3} + O(\epsilon^2) \tag{2.18}$$

while B is at $x = 0$, with radial location

$$y_B = \frac{\delta}{1+\delta} + \epsilon\frac{\delta(\delta^2-\delta+4)}{(1+\delta)^3} + O(\epsilon^2). \tag{2.19}$$

Clearly, A and B have the same radial location to leading order. Thus, in the concentric case with $\epsilon = 0$, the double homoclinic loop Γ collapses into a concentric ring at $y = \delta/(1+\delta)$, which is a degenerate circle of stagnation points. At $\delta = 0$ the flow consists of periodic orbits with no stagnation points and no turning points; there is no circulation region and every tracer particle winds around the inner cylinder.

Hence, at $\delta = 0$, both A and B are located at the outer wall and they move towards the inner wall as δ increases, with A always at $x = \pi$ and B at $x = 0$. At $\delta = 1$ the flow field has a high degree of symmetry: A is located dead centre at $x = \pi$ with $y_A = \frac{1}{2}(1-\epsilon)$ and B is located dead centre at $x = 0$ with $y_B = \frac{1}{2}(1+\epsilon)$. As δ increases beyond unity, A and B move slowly towards the inner wall and at $\delta \to \infty$ they are located at the inner wall.

As shown in figure 2, the family of closed streamlines around B converge to the separatrix Γ which is connected to the hyperbolic stagnation point A. This separatrix Γ is a double homoclinic loop of the fixed point A with the branch near the outer wall denoted as Γ_+ and the branch near the inner wall denoted as Γ_-. The Γ_+ loop in figure 2 is depicted with a stroboscopic map of a marked fluid element near A. As shown, there is considerable stretching as the fluid element departs the saddle points which is evident from the larger spacing. This stretching and a subsequent folding mechanism introduced by the homoclinic tangle are responsible for the Lagrangian chaos. We obtain an estimate of the radial location of either branch of Γ and, consequently, the width of the circulation region bounded by Γ, by expanding the steady stream function about $y_*(x)$. For every given azimuthal position, x, we expand $\bar{\psi}$ of (2.13) about $y_*(x)$ of (2.17)

$$\bar{\psi}(x,y) = \bar{\psi}(y_*) + (y-y_*)\frac{\partial \bar{\psi}}{\partial y}\bigg|_{y=y_*} + \tfrac{1}{2}(y-y_*)^2 \frac{\partial^2 \bar{\psi}}{\partial y^2}\bigg|_{y=y_*} + O((y-y_*)^3). \tag{2.20}$$

Expressing $y_*(x)$ as

$$y_*(x) = y_*^{(0)} + \epsilon y_*^{(1)}(x) + O(\epsilon^2) \tag{2.21}$$

where $y_*^{(0)}$ and $y_*^{(1)}$ are obtained from (2.17), we have from (2.20)

$$\bar{\psi}(x,y) = \bar{\psi}_0(y_*^{(0)}) + \tfrac{1}{2}(y-y_*)^2 \frac{\mathrm{d}^2 \bar{\psi}_0}{\mathrm{d}y^2}\bigg|_{y=y_*^{(0)}} + \epsilon \bar{\psi}_1(x, y_*^{(0)}) + O(\epsilon(y-y_*)^2) + O(\epsilon^2). \tag{2.22}$$

By stipulating that the stream function on the double homoclinic loop Γ must be identical to that at the hyperbolic point A, $\bar{\psi}(\pi, y_A)$, we obtain an expression for the width of the circulation bubble at every azimuthal position, x. We require, for any $(x, y_\pm)$ on Γ, where $y_\pm(x)$ is the radial location of the two branches of separatrix Γ,

$$\bar{\psi}(x, y_\pm) = \bar{\psi}(\pi, y_A), \tag{2.23}$$

and expressing y_A as

$$y_A = y_A^{(0)} + \epsilon y_A^{(1)}, \tag{2.24}$$

where $y_A^{(0)}$ and $y_A^{(1)}$ are obtained from (2.18)

$$\begin{aligned} \psi(\pi, y_A) &= \bar{\psi}_0(y_A) + \epsilon \bar{\psi}_1(\pi, y_A) \\ &= \bar{\psi}_0(y_A^{(0)}) + \epsilon \psi_1(\pi, y_A^{(0)}) + O(\epsilon^2). \end{aligned} \tag{2.25}$$

Since $y_*^{(0)} = y_A^{(0)}$, (2.23) gives

$$\begin{aligned} (y_\pm - y_*) &= \pm \epsilon^{\frac{1}{2}} \left[\frac{\bar{\psi}_1(\pi, y_A^{(0)}) - \bar{\psi}_1(x, y_A^{(0)})}{\frac{1}{2}\dfrac{\mathrm{d}^2 \bar{\psi}_0}{\mathrm{d}y^2}\Big|_{y=y_A^{(0)}}} \right]^{\frac{1}{2}} + O(\epsilon^{\frac{3}{2}}) \\ &= \pm \epsilon^{\frac{1}{2}} y_\Gamma(x, \delta) + O(\epsilon^{\frac{3}{2}}) \end{aligned} \tag{2.26}$$

where

$$y_\Gamma(x, \delta) = \frac{2\delta}{(1+\delta)^2}(1+\cos x)^{\frac{1}{2}}. \tag{2.27}$$

For any azimuthal position x, the radial coordinate of the separatrix Γ is then given by

$$y_{\pm}(x) = y_*^{(0)} \pm \epsilon^{\frac{1}{2}} y_\Gamma(x,\delta) + \epsilon y_*^{(1)} + O(\epsilon^{\frac{3}{2}}), \tag{2.28}$$

where the $\pm$ signs refer to the inner and outer branches of the double homoclinic loop respectively. It can be shown quite easily that the next term in (2.26) is indeed $O(\epsilon^{\frac{3}{2}})$, which explains the specific form of (2.28). Hence, the circulation region has a width of $O(\epsilon^{\frac{1}{2}})$ and the width at any azimuthal position, $W(x)$, is given by

$$W(x) = 2|y_{\pm}(x) - y_*(x)|, \tag{2.29}$$

which is, to leading order,

$$W(x) = 2\epsilon^{\frac{1}{2}} y_\Gamma(x,\delta) + O(\epsilon^{\frac{3}{2}}), \tag{2.30}$$

where $y_\Gamma(x,\delta)$ is given by (2.27). As expected, $W(x)$ vanishes at the narrowest part of the gap, $x = \pi$, and is maximum at the widest part of the gap, $x = 0$. Moreover, the width exhibits a maximum at a speed ratio of $\delta = 1$. To leading order in ϵ, y_A, y_B, y_* and $y_{\pm}$ are identically equal to $\delta/(1+\delta)$ and we shall refer to this quantity as y_s for convenience where s denotes stagnation.

A more accurate lubrication approximation, which involves an expansion only in the clearance λ and not the eccentricity ϵ, can be derived using the two-dimensional bipolar coordinates (ζ, η) instead of the present local Cartesian coordinates. Bipolar coordinates are a natural choice of coordinate system for planar flow between two eccentric cylinders since the boundaries are exactly represented by curves of constant η. To $O(\lambda^0)$, the velocity field in terms of the bipolar coordinates (ζ, η), where ζ is the azimuthal coordinate and η is the radial coordinate, are

$$u(\zeta,\eta,t) = \frac{P_\zeta \bar{\eta}}{\cosh\eta_0 - \cos\zeta}\left(\frac{\bar{\eta}-\bar{\eta}_1}{2}\right) + \delta(1+\alpha\sin\omega t)\left(\frac{\bar{\eta}}{\bar{\eta}_1}-1\right) + \frac{\bar{\eta}}{\bar{\eta}_1}, \tag{2.31}$$

$$v(\zeta,\eta,t) = \frac{P_\zeta \bar{\eta}^2 \sin\zeta}{(\cosh\eta_0 - \cos\zeta)^2}\left(\frac{\bar{\eta}}{3}-\frac{\bar{\eta}_1}{2}\right) - \frac{P_\zeta \bar{\eta}^2}{\cosh\eta_0 - \cos\zeta}\left(\frac{\bar{\eta}}{6}-\frac{\bar{\eta}_1}{4}\right)$$
$$+ \frac{\sin\zeta}{(\cosh\eta_0 - \cos\zeta)}\left[\frac{\bar{\eta}^2}{2\bar{\eta}_1} + \delta(1+\alpha\sin\omega t)\left(\frac{\bar{\eta}}{2\bar{\eta}_1}-1\right)\bar{\eta}\right], \tag{2.32}$$

where, at $\lambda \to 0$, the inner wall is represented by $\eta = \eta_1$, the outer wall by $\eta = \eta_0$, and

$$\bar{\eta} = \eta - \eta_0, \tag{2.33}$$

$$\bar{\eta}_1 = \eta_1 - \eta_0. \tag{2.34}$$

The derivatives of pressure, p, with respect to the azimuthal variable are

$$p_\zeta = \frac{-6}{\bar{\eta}_1^2}[1-\delta(1+\alpha\sin\omega t)][\cos\zeta + a_2 \tfrac{1}{2}\{\cos 2\zeta\} - 2\cosh\eta_0\cos\zeta)], \tag{2.35}$$

$$p_{\zeta\zeta} = \frac{-6}{\bar{\eta}_1^2}[1-\delta(1+\alpha\sin\omega t)][-\sin\zeta + a_2(-\sin 2\zeta)], \tag{2.36}$$

$$a_2 = \frac{2\cosh\eta_0}{1+2\cosh^2\eta_0}. \tag{2.37}$$

We shall use the simpler Cartesian version of (2.10) and (2.11) in our asymptotic analysis of the heat-transfer problem. The more accurate expressions in (2.31) and

(2.32) will be reserved for the numerical studies and simulations of the flow. It can be easily verified that in the limit of small eccentricity, ϵ, the two flow fields become identical.

3. Steady enhancement at high Pe

We shall study the enhancement in heat/mass transfer in terms of an effective diffusion coefficient, like a Nusselt number, for time and azimuthally averaged diffusion flux across the gap in the radial direction. The coefficient of effective diffusion is normalized with respect to the diffusivity, D. We define

$$\frac{\langle \bar{D}_{\text{eff}} \rangle}{D} = \frac{\langle \bar{Q}_{\text{total}} \rangle}{\langle \bar{Q}_{\text{conduction}} \rangle}, \tag{3.1}$$

where a bar denotes integral over the azimuthal direction and $\langle\ \rangle$ denotes time-averaging. The quantity $\langle \bar{Q}_{\text{total}} \rangle$ is the time-averaged total heat flux across the gap and $\langle \bar{Q}_{\text{conduction}} \rangle$ is the corresponding quantity in the absence of convection for concentric cylinders. Therefore, $\langle \bar{D}_{\text{eff}}/D \rangle$ is unity for a concentric cylinder. Note that $\langle \bar{D}_{\text{eff}} \rangle$ is appropriate only after the initial transients have died and the flux is either steady or time-periodic. For simplicity, we shall abuse notation and use $\bar{D}_{\text{eff}}$ to represent the steady effective diffusion.

The dimensionless energy equation can also be simplified by a lubrication approximation which exploits the small clearance of the gap. To $O(\lambda^0)$ and in local Cartesian coordinates, it becomes

$$\frac{\partial T}{\partial t} + u\frac{\partial T}{\partial x} + v\frac{\partial T}{\partial y} = \frac{1}{Pe}\frac{\partial^2 T}{\partial y^2} + O(\lambda^2), \tag{3.2}$$

where the dimensionless T is related to the dimensional one, $\hat{T}$, by

$$T = \frac{\hat{T} - T_{\text{i}}}{T_{\text{o}} - T_{\text{i}}}, \tag{3.3}$$

and, T_{i} and T_{o} are the temperatures at the inner and outer walls respectively, with $T_{\text{o}} > T_{\text{i}}$ for convenience. The Péclet number, Pe, is $c^2\omega_{\text{i}}/D$. The pertinent boundary conditions are then

$$T(y = 0) = 1, \tag{3.4}$$

$$T(y = h) = 0. \tag{3.5}$$

At steady state (3.2) reduces to

$$\bar{u}\frac{\partial T}{\partial x} + \bar{v}\frac{\partial T}{\partial y} = \frac{1}{Pe}\frac{\partial^2 T}{\partial y^2} + O(\lambda^2) \tag{3.6}$$

with the same boundary conditions.

Both the steady and perturbed flow fields yield insignificant enhancement at low Pe. A regular perturbation in Pe produces the classical result of $\bar{D}_{\text{eff}} = D(1 + a\,Pe^2)$ for both steady and time-averaged enhancement where a is a constant depending on system geometry (Ghosh 1991). This is quite different, however, at high Pe. Batchelor (1956) has suggested that, at high Péclet numbers, the steady-state temperature field within a separated recirculation region like Ω_{i} is completely

uniform owing to fast mixing along the streamlines. Similar studies have been carried out by Rhines & Young (1983) and Young, Pumir & Pomeau (1989). We shall show that, after proper rescaling, this is also true of the present system and different expansions are then required for inside and outside Ω_1. We shall carry out a leading-order asymptotic expansion of the steady-transport equation both in the diffusion dominant outer regions and the advection dominant recirculation region. The expansions are then matched at the separatrices where azimuthal advection matches radial diffusion.

3.1. *Recirculation region*

The scalings leading to (3.6) are appropriate only for the outer Ω_1 and Ω_2 regions where conduction dominates. Within the recirculation region Ω_i, the velocity scales and lengthscales are different Péclet number results. Linearizing the steady flow field about the elliptic stagnation point, B, yields a pair of purely imaginary eigenvalues

$$\lambda_{1,2} = \pm i\sqrt{2}\,\epsilon^{\frac{1}{2}}\frac{\delta}{1+\delta} + O(\epsilon), \tag{3.7}$$

which indicates that the circulation around B becomes more rapid with increasing ϵ and δ. Solving for the eigenvectors associated with the eigenvalues of (3.7) yields the following parametric dependence of the steady flow, $\bar{u}$ and $\bar{v}$, in the vicinity of B

$$\bar{u} \sim \epsilon^{\frac{1}{2}}\delta, \tag{3.8a}$$

$$\bar{v} \sim \frac{\epsilon\delta^2}{(1+\delta)^2}. \tag{3.8b}$$

Clearly, for arbitrarily small ϵ or arbitrarily small δ, the recirculation bubble is no longer a well-mixed region at steady state. Equations (3.8) suggest rescaling $\bar{u}$ and $\bar{v}$ into the new scaled variables $\tilde{u}$ and $\tilde{v}$,

$$\tilde{u} = \bar{u}/\epsilon^{\frac{1}{2}}\delta, \tag{3.9a}$$

$$\tilde{v} = \bar{v}\Big/\frac{\epsilon\delta^2}{(1+\delta)^2}. \tag{3.9b}$$

Equations (3.7) and (3.8) also provide the appropriate lengthscales in the vicinity of B. They are

$$\tilde{x} = x, \tag{3.10a}$$

$$\tilde{y} = y\Big/\frac{\epsilon^{\frac{1}{2}}\delta}{(1+\delta)^2}. \tag{3.10b}$$

This is consistent with the width of the recirculation bubble, as given by $W(x)$ of (2.30), which also varies as $\epsilon^{\frac{1}{2}}\delta/(1+\delta)^2$. The rescaled steady-state energy equation within the recirculation region Ω_1 is then

$$\tilde{u}\frac{\partial T}{\partial \tilde{x}} + \tilde{u}\frac{\partial T}{\partial \tilde{y}} = \frac{1}{\tilde{P}e}\frac{\partial^2 T}{\partial \tilde{y}^2}, \tag{3.11}$$

where $\tilde{P}e$ is the appropriate Péclet number within Ω_1 and is related to the global Péclet number, Pe, by

$$\tilde{P}e = \frac{\epsilon^{\frac{3}{2}}\delta^3}{(1+\delta)^4}Pe. \tag{3.12}$$

We shall carry out the expansion in $1/\tilde{Pe}$ which then stipulates that $Pe \gg \epsilon^{-\frac{3}{4}}\delta^{-3}$. The leading-order equation within Ω_1 in the limit of $1/\tilde{Pe}$ approaching zero is then

$$\tilde{u}\frac{\partial T}{\partial \tilde{x}}+\tilde{v}\frac{\partial T}{\partial \tilde{y}} = -\frac{\partial \tilde{\psi}}{\partial \tilde{y}}\frac{\partial T}{\partial \tilde{x}}+\frac{\partial \tilde{\psi}}{\partial \tilde{x}}\frac{\partial T}{\partial y} = \boldsymbol{z}\cdot(\boldsymbol{\nabla}\tilde{\psi}\times\boldsymbol{\nabla}T)$$
$$= 0, \tag{3.13}$$

where $\boldsymbol{z}$ is the unit normal perpendicular to the (x, y)-plane and $\tilde{\psi}$ is the steady-state stream function in Ω_1. Hence, the streamlines are identical to the isotherms and T is a function of $\tilde{\psi}$ only to leading order,

$$T = T(\tilde{\psi}). \tag{3.14}$$

However, integrating the steady-state energy equation over the domain interior to a closed streamline L with streamfunction $\tilde{\psi}_0$ and invoking the divergence theorem yields

$$\oint_L \boldsymbol{n}\cdot\boldsymbol{\nabla}T\,\mathrm{d}l = 0. \tag{3.15}$$

Since, at steady state, there is no accumulation and no convection across L, the total diffusive flux must then vanish exactly. However, $\boldsymbol{\nabla}T = (\mathrm{d}T/\mathrm{d}\tilde{\psi})\boldsymbol{\nabla}\tilde{\psi}$ from (3.14) and the zero flux conditions of (3.15) yields

$$\oint_L \boldsymbol{n}\cdot\tilde{\psi}\frac{\mathrm{d}T}{\mathrm{d}\tilde{\psi}}\mathrm{d}l = \left.\frac{\mathrm{d}T}{\mathrm{d}\tilde{\psi}}\right|_{\tilde{\psi}=\tilde{\psi}_0}\oint_L \boldsymbol{n}\cdot\boldsymbol{\nabla}\tilde{\psi}\,\mathrm{d}l = 0, \tag{3.16}$$

since $\tilde{\psi} = \tilde{\psi}_0$ along L. Because the unit normal $\boldsymbol{n}$ is $\boldsymbol{\nabla}\tilde{\psi}/|\boldsymbol{\nabla}\tilde{\psi}|$, the line integral $\oint_L \boldsymbol{n}\cdot\boldsymbol{\nabla}\tilde{\psi}\,\mathrm{d}l$ is simply $\oint_L|\boldsymbol{\nabla}\tilde{\psi}|\,\mathrm{d}l$ which is non-zero. Consequently,

$$\left.\frac{\mathrm{d}T}{\mathrm{d}\tilde{\psi}}\right|_{\tilde{\psi}=\tilde{\psi}_0}$$

must vanish and the normal temperature gradient vanishes at every point on L. Since L can be any arbitrary closed streamline, T must be uniform in the interior of Ω_1. The above is just a mathematical delineation of the physical fact that any steady-temperature field which depends only on the streamfunction must be uniform within a closed streamline. Since, at high $\tilde{Pe}$, the temperature within Ω_1 is constant, it must be equal to the temperature at the hyperbolic stagnation point A. Consequently, at large $\tilde{Pe}$, the temperature within Ω_1 is equal to that at the hyperbolic stagnation point to leading order and at steady state.

3.2. *Outer diffusive regions*

We shall also carry out a leading-order analysis of the Ω_1 and Ω_2 regions with nearly parallel flow. Expanding T as

$$T = T_0+\epsilon T_1+\ldots, \tag{3.17}$$

the energy equation (3.6) yields to $O(\epsilon^0)$,

$$\bar{u}_0(y)\frac{\partial T_0}{\partial x} = \frac{1}{Pe}\frac{\partial^2 T_0}{\partial y^2}+O(\epsilon), \tag{3.18}$$

where $\bar{u}_0$ is given in (2.10) and the original scalings of §2 are appropriate here. Equation (3.18) is valid for all orders in Pe^{-1}. However, regardless of the magnitude

of Pe^{-1}, the only solution to (3.18), in both Ω_1 and Ω_2, is a purely conductive temperature profile linear in y. We have hence shown that the local radial temperature profiles at every azimuthal position x are linear in the Ω_1 and Ω_2 regions in spite of the high convective contribution. This is because the convection is orthogonal to the direction of heat flux to leading order here. Since, to leading order in the eccentricity, both Ω_1 and Ω_2 are diffusion dominant parallel flow regions with a linear conductive temperature profile, the temperature at the hyperbolic point A, denoted by T_1, is easily obtained

$$T_1 = T_0(x=\pi, y=y_A) = 1-\frac{y_A}{1-\epsilon} = 1-y_s+O(\epsilon) = \frac{1}{1+\delta}+O(\epsilon), \tag{3.19}$$

where, to be consistent in our resolution, we omit the $O(\epsilon)$ term and $y_s = \delta/(1+\delta)$ is the leading-order estimate of the radial location of A in (2.18).

3.3. *Zero-order estimate of steady enhancement*

A zeroth-order theory for steady enhancement can immediately be obtained from the previous leading-order analysis of the convectively dominant Ω_1 and the diffusivity dominant Ω_1 and Ω_2. Imposing boundary conditions (3.4) and (3.5) and using (2.28) to estimate the radial location of separatrix Γ, one gets at every azimuthal position, the profile

$$T(x,y) = 1-\frac{y}{y_+}(1-T_1) \quad (0<y<y_+), \tag{3.20a}$$

$$T(x,y) = T_1 \qquad (y_+ \leqslant y \leqslant y_-), \tag{3.20b}$$

$$T(x,y) = T_1\frac{(h-y)}{(h-y_-)} \qquad (y_- < y < h), \tag{3.20c}$$

where y_+ and y_- are the boundaries Γ of the circulation region Ω_1 of (2.28) and h of (2.9) gives the location of the inner wall. We shall only retain $O(\epsilon^{\frac{1}{2}})$ terms in $y_\pm(x)$ of (2.28) in the leading estimate. Thus

$$y_+ = y_s-\epsilon^{\frac{1}{2}}y_\Gamma(x,\delta)+O(\epsilon), \tag{3.21a}$$

$$y_- = y_s+\epsilon^{\frac{1}{2}}y_\Gamma(x,\delta)+O(\epsilon), \tag{3.21b}$$

and

$$h = 1+O(\epsilon). \tag{3.21c}$$

It is evident that the uniform region in Ω_1 will enhance the flux by an amount which varies as $\epsilon^{\frac{1}{2}}$. This can be easily summarized by a steady enhancement defined in terms of effective diffusivity, as in (3.1), and denoted here by $\bar{D}^\infty_{\text{eff}}/D$,

$$\frac{\bar{D}^\infty_{\text{eff}}}{D} = 1+\frac{\epsilon^{\frac{1}{2}}}{2\pi\, y_s}\int_0^{2\pi} y_\Gamma(x,\delta)\,\mathrm{d}x+O(\epsilon). \tag{3.22}$$

Inserting y_Γ from (2.27), we obtain the steady enhancement to $O(\epsilon^{\frac{1}{2}})$ in the eccentricity,

$$\frac{\bar{D}^\infty_{\text{eff}}}{D}(\epsilon,\delta) = 1+\frac{\epsilon^{\frac{1}{2}}4\sqrt{2}}{\pi(1+\delta)}+O(\epsilon). \tag{3.23}$$

We note that $\tilde{P}e$ is the appropriate Péclet number in Ω_1 and (3.23) holds only for $\tilde{P}e\to\infty$. Consequently, from (3.12), (3.23) does not hold in the limit of $\epsilon\to 0$ or $\delta\to 0$. From §2, we know that at $\delta = 0$ all trajectories in the steady flow wind around the

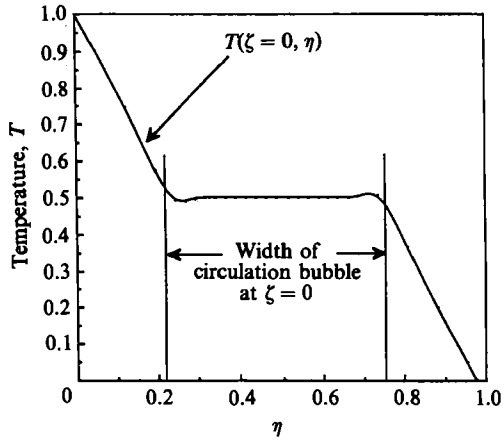

FIGURE 3. The numerically computed temperature profile at the largest clearance ($\zeta = x = 0$) in the bipolar coordinate. The outer wall is at $\eta = 0$ and the inner wall $\eta = 1$. The recirculation region Ω_1 is also indicated. Note the diffusive boundary layers lie on the Ω_1 side of Γ. Parameter values are $Pe = 5000$, $\epsilon = 0.2$ and $\delta = 1.0$.

inner cylinder and thus there is no enhancement irrespective of the magnitude of Pe, or $\tilde{P}e$, i.e. $(\bar{D}^{\infty}_{\rm eff}/D)|_{\delta=0} = 1$. Equation (3.23) does not reduce to this result in the asymptotic limit of $\delta \to 0$ because $\delta \to 0$ is not a valid limit at large $\tilde{P}e$.

If we include the $O(\epsilon)$ terms in T_1, then

$$T_1 = 1 - y_s - \epsilon(y_A^{(0)} + y_A^{(1)}) + O(\epsilon^2), \tag{3.24}$$

where both $y_A^{(0)}$ and $y_A^{(1)}$ are obtained from (2.18). If we also include the $O(\epsilon)$ contributions from $y_+(x)$ and $y_-(x)$ in (2.28) and $h(x)$ of (2.9), then the steady enhancement to zeroth order in $1/\tilde{P}e$ and to $O(\epsilon)$ is

$$\frac{\bar{D}^{\infty}_{\rm eff}}{D} = 1 + \epsilon^{\frac{1}{2}} \frac{4\sqrt{2}}{\pi(1+\delta)} + \epsilon\left[1 - \frac{4\sqrt{2}}{\delta\pi} + \frac{(\delta^2 - \delta + 4)}{(1+\delta)^2}\right] + O(\epsilon^{\frac{3}{2}}). \tag{3.25}$$

In figure 3, we depict the temperature profile at $x = 0$, computed with a finite difference scheme from the energy equation using the more accurate bipolar flow fields of (2.31) and (2.32) with $Pe = 5000$ which yields a $\tilde{P}e = 27.95$ for $\epsilon = 0.2$ and $\delta = 1.0$ of figure 3. Owing to the instability of the finite-difference scheme for nearly hyperbolic systems, we are unable to increase Pe or $\tilde{P}e$ further. As evident, however, the estimated profile of (3.20) provides a satisfactory leading-order approximation of the actual values in spite of this relatively low $\tilde{P}e$. At the conditions of figure 3, the hyperbolic stagnation point is located dead centre to leading order in ϵ at $x = \pi$ with $y_A = y_s = 0.5$. Thus, the temperature T_1 at this stagnation point is estimated to be 0.5 by (3.19). From figure 3, it is clearly evident that the uniform temperature within Ω_1 is indeed equal to T_1 and extends almost right across the width of Ω_1 at this azimuthal position of $x = 0$. This validates the predictions of our zeroth-order theory.

3.4. *Boundary-layer analysis and higher-order estimates*

Two boundary layers are clearly evident in figure 3 on the interior of Γ_+ and Γ_- (their radial locations are marked by two straight lines) where the conductive regions Ω_1 and Ω_2 meet the convective regions Ω_1. In these boundary layers the regular perturbation solution of (3.11) breaks down as the right-hand side of the equation

contributes significantly within this narrow layer interior and adjacent to Γ. Here derivatives with respect to $\tilde{y}$ become large in order that the zero first derivative of temperature well within Ω_1 matches to a finite but constant value in Ω_1 and Ω_2. In physical terms, since there is a finite uniform flow along Γ, conduction normal to the streamlines is balanced by streamwise convection in these boundary layers as in boundary layers beneath a mobile surface (Shraiman 1987). Consequently, the 'dominant balance' arguments (see Stewart 1977) yield a boundary-layer thickness of $Pe^{-\frac{1}{2}}$ along Γ. In the subsequent boundary-layer analysis, we shall resolve these diffusive boundary layers to improve the estimate of enhancement in (3.23) by obtaining the first correction due to a large but finite $\tilde{P}e$. We shall, however, carry out the expansion in Pe^{-1} since the velocity scalings of the parallel flow regions are more appropriate in the boundary layers. To ensure a gradientless circulation region, it will be understood in what follows that ϵ and δ must have sufficiently large values such that $\tilde{P}e$ is also large. We rescale the local Cartesian coordinate normal to the streamlines by $Pe^{-\frac{1}{2}}$ for the boundary layers. Since Γ only exists for eccentric cylinders, the location of the separatrix varies with x and care must be taken to account for its $\epsilon^{\frac{1}{2}}$ x-dependence. We introduce a rescaled normal coordinate defined by the steady stream function $\bar{\psi}$, valid to $O(\epsilon)$.

$$\sigma = Pe^{\frac{1}{2}}(\bar{\psi} - \bar{\psi}_\Gamma), \tag{3.26}$$

where $\bar{\psi}_\Gamma$ is the stream function on Γ and at the hyperbolic point A, $\bar{\psi}_\Gamma = \bar{\psi}(\pi, y_A)$, and $\sigma\epsilon[0, \infty)$. The tangential coordinate τ is defined by

$$\mathrm{d}\tau = -\frac{\partial\bar{\psi}}{\partial y}\mathrm{d}x + \frac{\partial\bar{\psi}}{\partial x}\mathrm{d}y. \tag{3.27}$$

In terms of this local Cartesian coordinate along Γ, the steady-state energy equation of (3.6), where $\bar{u}$ and $\bar{v}$ are valid to $O(\epsilon)$, becomes

$$\frac{\partial T}{\partial\tau}|\nabla\bar{\psi}|^2 = \frac{\partial^2 T}{\partial\sigma^2}\left(\frac{\partial\bar{\psi}}{\partial y}\right)^2 + Pe^{-\frac{1}{2}}\left(\frac{\partial T}{\partial\sigma}\frac{\partial^2\bar{\psi}}{\partial y^2} + 2\frac{\partial^2 T}{\partial\sigma\delta\tau}\frac{\partial\bar{\psi}}{\partial y}\frac{\partial\tau}{\partial y}\right) + O(Pe^{-1}). \tag{3.28}$$

The metrics $|\nabla\bar{\psi}|^2$, $\partial\bar{\psi}/\partial y$, $(\partial^2\bar{\psi}/\partial y^2)$ and $\partial\tau/\partial y$ are all evaluated along Γ. From (2.13), it can be readily seen that

$$\frac{\partial\bar{\psi}}{\partial x} \sim O(\epsilon), \tag{3.29}$$

and hence $(\partial\bar{\psi}/\partial x)^2$ is $O(\epsilon^2)$ and can be omitted. Consequently (3.28) reduces to

$$\left(\frac{\partial\bar{\psi}}{\partial y}\right)^2\frac{\partial T}{\partial\tau} = \frac{\partial^2 T}{\partial\sigma^2}\left(\frac{\partial\bar{\psi}}{\partial y}\right)^2 + Pe^{-\frac{1}{2}}\left[\frac{\partial T}{\partial\sigma}\frac{\partial^2\bar{\psi}}{\partial y^2} + 2\frac{\partial^2 T}{\partial\sigma\,\partial\tau}\frac{\partial\bar{\psi}}{\partial y}\frac{\partial\tau}{\partial y}\right] + O(Pe^{-1}) + O(\epsilon). \tag{3.30}$$

Close to the separatrix Γ, $\bar{\psi}$ can be linearized in y to give

$$\bar{\psi} = \bar{\psi}_\Gamma + \phi_\Gamma(x)\,(y - y_\pm(x)), \tag{3.31}$$

where $y_\pm(x)$ gives the radial location of separatrix Γ, and

$$\phi_\Gamma(x) = \left.\frac{\partial\bar{\psi}}{\partial y}\right|_\Gamma \sim \left.\frac{\mathrm{d}\bar{\psi}_0}{\mathrm{d}y}\right|_{y=y_\pm(x)} + O(\epsilon). \tag{3.32a}$$

Inserting $y_\pm(x)$ from (2.28)

$$\phi_\Gamma(x) = \epsilon^{\frac{1}{2}}\phi_{\frac{1}{2}}(x) + O(\epsilon), \tag{3.32b}$$

where $$\phi_{\frac{1}{2}}(x) = \pm\frac{2\delta}{(1+\delta)}(1+\cos x)^{\frac{1}{2}}, \tag{3.32c}$$

and the $\pm$ signs refer to the outer and inner branches of the double homoclinic loop Γ, respectively. From (3.27), (3.29) and (3.32)

$$\tau = -\int_{\pi}^{x} \epsilon^{\frac{1}{2}}\phi_{\frac{1}{2}}(x')\,\mathrm{d}x' + O(\epsilon) \tag{3.33a}$$

$$= \begin{cases} \pm\dfrac{4\sqrt{2\delta}}{1+\delta}\epsilon^{\frac{1}{2}}(1-\sin\tfrac{1}{2}x) + O(\epsilon) & (0 \leqslant x \leqslant \pi) \qquad (3.33b) \\ \pm\dfrac{4\sqrt{2\delta}}{1+\delta}\epsilon^{\frac{1}{2}}(\sin\tfrac{1}{2}x - 1) + O(\epsilon) & (\pi \leqslant x \leqslant 2\pi), \qquad (3.33c) \end{cases}$$

where the hyperbolic stagnation point A is chosen to be the origin of τ. Once again, the $\pm$ signs correspond to Γ_+ and Γ_- respectively.

The boundary-layer equation of (3.30) resembles a transient diffusion equation to leading order. In the normal directions, its solutions must match into the uniform field in the interior of Ω_1 and the linear profiles of (3.20*a*) and (3.20*c*) in Ω_1 and Ω_2. For simplicity, we shall detail only the resolution of the outer boundary layer along Γ_+. The normal boundary conditions there are then

$$\left.\frac{\partial T}{\partial \sigma}\right|_{\sigma\to\infty} = 0, \tag{3.34a}$$

$$\left.\frac{\partial T}{\partial \sigma}\right|_{\sigma=0} = \frac{Pe^{-\frac{1}{2}}}{\phi_{\Gamma_+}(x)\,y_+(x)}(T(\sigma=0)-1). \tag{3.34b}$$

In (3.34*b*), $(T(\sigma=0)-1)/y_+(x)$ is simply the slope of the linear diffusive profile in Ω_1 since $y_+(x)$ is the width of Ω_1. This then must be equated to $\partial T/\partial y$ in the diffusive boundary layer which is $\phi_{\Gamma_+} Pe^{\frac{1}{2}}\,(\partial T/\partial\sigma)$ through the scalings of (3.26) and (3.31). Since we are interested in only the leading-order contribution of the eccentricity ϵ at every order of the expansion in Pe^{-1}, we shall retain only those terms in the boundary layer equations which contribute to leading order in ϵ. Thus, expanding (3.34*b*) in ϵ after substituting (2.28), one obtains

$$\left.\frac{\partial T}{\partial \sigma}\right|_{\sigma=0} = \frac{Pe^{-\frac{1}{2}}\epsilon^{-\frac{1}{2}}}{\phi_{\frac{1}{2}}(x)\,y_s}\left[1+\frac{\epsilon^{\frac{1}{2}}y_\Gamma(x,\delta)}{y_s}\right](T(\sigma=0)-1), \tag{3.35}$$

where $\phi_{\frac{1}{2}}(x)$ is given by (3.32*c*), y_Γ by (2.27) and $y_s = \delta/(1+\delta)$ is simply the leading-order estimate of y_A. We note that while the second $\epsilon^{\frac{1}{2}}$ term in the square bracket is much smaller than the unity first term, it must be retained to include the effect of the recirculation region. The first term, to leading order in Pe^{-1}, will simply yield the unit flux of the purely diffusive linear profile after proper transform to the y-coordinate.

The width of the circulation bubble, $W(x)$ of (2.30), is a function of azimuthal position x and is zero at the hyperbolic stagnation point A at $x = \pi$. Consequently, there is an azimuthal neighbourhood of $x = \pi$ where the circulation region is of negligible width and the linear profiles of (3.20) extend right across. However, we cannot determine the width of this azimuthal neighbourhood, $|x=\pi|$, since the width $W(x)$ decreases very rapidly to zero as we approach $x = \pi$ from either side. In fact, $\mathrm{d}W(x)/\mathrm{d}x$ approaches infinity at $x = \pi$. Consequently, there is an infinitesimal

azimuthal neighbourhood near A, whose size we cannot determine, where the circulation is negligible and the linear profiles, (3.18a) and (3.18c) in Ω_1 and Ω_2, collapse into one continuous linear profile extending from the outer to the inner wall. Hence, to match the boundary-layer solution T of (3.30) to the 'initial' boundary layer near A, one must have

$$T(\tau = 0) = T_i \tag{3.36}$$

given, to leading order, by (3.19).

Equation (3.30) with 'initial' and boundary conditions (3.34)–(3.36), which are valid to $O(\epsilon^{\frac{1}{2}})$ and $O(Pe^{-\frac{1}{2}})$, can be easily solved with an expansion in $Pe^{-\frac{1}{2}}$,

$$T \sim T_0 + T_{\frac{1}{2}} Pe^{-\frac{1}{2}} + T_1 Pe^{-1} + \ldots. \tag{3.37}$$

Here T_0 is the leading-order term in the expansion within the boundary layer in Ω_1 and should not be confused with T_0 of (3.18) which denotes the leading term within Ω_1 and Ω_2. The leading-order equations,

$$\frac{\partial T_0}{\partial \tau} = \frac{\partial^2 T_0}{\partial \sigma^2}, \tag{3.38}$$

$$T_0(\tau = 0) = 1 - y_s, \tag{3.39a}$$

$$\frac{\partial T_0}{\partial \sigma}(\sigma \to \infty) = 0, \tag{3.39b}$$

$$\frac{\partial T_0}{\partial \tau}(\sigma = 0) = 0, \tag{3.39c}$$

simply yields the uniform temperature profile $T_0 = 1/1 + \delta = 1 - y_s$ of (3.19) in our previous leading-order analysis. In fact, in the present analysis, the flux is identically zero as indicated in (3.39c). To obtain the correct flux, we proceed to the next order, $O(Pe^{-\frac{1}{2}})$,

$$\frac{\partial T_{\frac{1}{2}}}{\partial \tau} = \frac{\partial^2 T_{\frac{1}{2}}}{\partial \sigma^2}, \tag{3.40a}$$

$$T_{\frac{1}{2}}(\tau = 0) = 0, \tag{3.40b}$$

$$\frac{\partial T_{\frac{1}{2}}}{\partial \sigma}(\sigma \to \infty) = 0, \tag{3.40c}$$

$$\begin{aligned} \frac{\partial T_{\frac{1}{2}}}{\partial \sigma}(\sigma = 0) &= \frac{\epsilon^{-\frac{1}{2}}}{\phi_{\frac{1}{2}}(x)\, y_s}\left[1 + \frac{\epsilon^{\frac{1}{2}} y_\Gamma}{y_s}\right](T_0 - 1), \\ &= \frac{-1}{\epsilon^{\frac{1}{2}} \phi_{\frac{1}{2}}(x)}\left[1 + \frac{\epsilon^{\frac{1}{2}} y_\Gamma}{y_s}\right]. \end{aligned} \tag{3.40d}$$

It is clear from (3.40c) that the first unity term in the square bracket corresponds to the purely diffusive flux while the second term yields the leading-order effect of the recirculation region. Upon integration over the entire gap, one simply obtains the previous result of (3.22). The effect of diffusive boundary layer still has not entered the analysis. This must now be contained in the T_1 equation whose boundary condition at $\sigma = 0$ is simply

$$\frac{\partial T_1}{\partial \sigma}(\sigma = 0) = \frac{\epsilon^{-\frac{1}{2}}}{\phi_{\frac{1}{2}}(x)\, y_s} T_{\frac{1}{2}}(\sigma = 0). \tag{3.41}$$

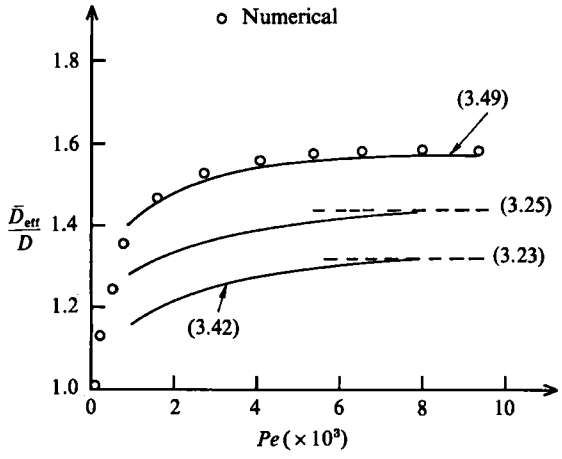

FIGURE 4. Comparison of the estimated steady enhancement at varying degree of resolution to numerical values at $\epsilon = 0.2$ and $\delta = 1.5$. Estimate (3.23) is the asymptotic enhancement at infinite Pe valid to $O(\epsilon)$. estimate (3.25) is the same value correct to $O(\epsilon^{\frac{3}{2}})$. Estimate (3.42) describes the $Pe^{-\frac{1}{2}}$ decay from the asymptote valid to $O(\epsilon, \epsilon^{\frac{1}{2}}Pe^{-\frac{1}{2}}, Pe^{-1})$ and the shift up improves its accuracy to $O(\epsilon^{\frac{3}{2}}, \epsilon^{\frac{1}{2}}Pe^{-\frac{1}{2}}, Pe^{-1})$. The estimate (3.49) is a more tedious 'expansion' valid to $O(\epsilon^2)$ and $O(Pe^{-1})$.

We have omitted the higher-order terms in ϵ in this Pe^{-1} order. The leading-order ϵ term is already contained in (3.40*c*). The effective steady enhancement is then obvious from (3.40*c*) and (3.41)

$$\frac{\bar{D}_{\text{eff}}}{D} = 1 + \frac{\epsilon^{\frac{1}{2}}}{2\pi y_s}\int_0^{2\pi} y_\Gamma \,\mathrm{d}x - \frac{Pe^{-\frac{1}{2}}}{2\pi y_s}\int_0^{2\pi} T_{\frac{1}{2}}(\sigma = 0)\,\mathrm{d}x + O(\epsilon) + O(Pe^{-1}) + O(\epsilon^{\frac{1}{2}}Pe^{-\frac{1}{2}})$$

$$\sim 1 + \frac{\epsilon^{\frac{1}{2}}4\sqrt{2}}{\pi(1+\delta)} - \frac{Pe^{-\frac{1}{2}}(1+\delta)}{2\pi\delta}\int_0^{2\pi} T_{\frac{1}{2}}(\sigma = 0)\,\mathrm{d}x. \quad (3.42)$$

Comparing to (3.23), it is clear that the third term in (3.42) determines the contribution of the diffusive boundary layers and it specifies that the enhancement decays by $Pe^{-\frac{1}{2}}$ from the infinite Pe asymptote of (3.23).

Quantitative evaluation of this term requires the solution of $T_{\frac{1}{2}}(\tau, \sigma)$ in (3.40). This can be easily achieved by the usual Green function technique

$$T_{\frac{1}{2}}(\tau, \sigma) = \frac{2}{\pi^{\frac{1}{2}}}\int_\sigma^\infty \mathrm{d}\xi \int_{\xi/2\tau^{\frac{1}{2}}}^\infty \mathrm{d}\mu f\left(\tau - \frac{\xi^2}{4\mu^2}\right)\exp(-\mu^2), \quad (3.43a)$$

where

$$f(x(\tau)) = \frac{[1 + \epsilon^{\frac{1}{2}}y_\Gamma(x)/y_s]}{\epsilon^{\frac{1}{2}}\phi_{\frac{1}{2}}(x)}, \quad (3.43b)$$

and $x(\tau)$ is obtained by inverting (3.33). It is then an easy matter to compute

$$\int_0^{2\pi} T_{\frac{1}{2}}(\sigma = 0)\,\mathrm{d}x$$

from (3.43). (In fact, the $\epsilon^{\frac{1}{2}}y_\Gamma(x)$ term can be safely neglected in (3.43*b*) but since the resulting integral must still be evaluated numerically, we retain it for completeness.) In figure 4, we compare the predictions by (3.42) to our finite-difference solution of the steady-state energy equation (3.6) in bipolar coordinates with flow fields (2.31)

and (2.32) for $\epsilon = 0.2$ and $\delta = 1.5$. It is clear from the figure that the enhancement approaches the asymptote 1.32 predicted by (3.23). The numerical result follows the same trend but is off by a constant value of approximately $O(\epsilon)$ at large Pe. If we include the $O(\epsilon)$ correction of (3.25) to (3.42), the error is reduced to $O(\epsilon^{\frac{3}{2}})$ at large Pe as expected. The asymptote in this case is 1.43 and the two curves are simply shifted by the ϵ term in (3.25) which is 0.11 for the geometry in question. This approach to a constant asymptote at high Pe as distinct from unbounded heat-transfer problems controlled by a diffusive boundary layer where a $Pe^{\frac{1}{2}}$ behaviour appears for a mobile surface and $Pe^{\frac{1}{3}}$ as asymptote exists for a solid one.

We conclude this section by obtaining a more accurate estimate of $\bar{D}^{\infty}_{\text{eff}}/D$ by employing a higher-order estimate of the boundary-layer equation (3.30) in ϵ. Here, we do not employ the $\epsilon^{\frac{1}{2}}$ estimate of the separatrices and the location of the hyperbolic stagnation point y_A but instead use the values from the steady flow of $\bar{\psi}$ in (2.13) which is valid to $O(\epsilon)$. However, this higher resolution in ϵ necessitates a numerical solution instead of the convenient closed-form solutions of (3.32), (3.25) and (3.42). The flux at the wall is now given by

$$-\frac{\partial T}{\partial y}\bigg|_{y=0} = \frac{1-T_{\text{i}}}{y_+(x)}\left(1-Pe^{-\frac{1}{2}}\frac{T_{\frac{1}{2}}(\sigma=0)}{1-T_{\text{i}}}\right), \tag{3.44}$$

where $T_{\frac{1}{2}}(\tau,\sigma)$ is given by (3.43), with

$$f[\tau(x)] = \frac{T_{\text{i}}-1}{y_+(x)\dfrac{\partial\bar{\psi}}{\partial y}\bigg|_{y=y_+(x)}}, \tag{3.45}$$

$$\tau(x) = -\int_{\pi}^{x}\frac{\partial\bar{\psi}}{\partial y}\bigg|_{y=y_+(x)}\mathrm{d}x, \tag{3.46}$$

$$T_{\text{i}} = 1-\frac{y_A}{1-\epsilon}. \tag{3.47}$$

The enhancement, $\bar{D}_{\text{eff}}/D$, is then given by

$$\frac{D_{\text{eff}}}{D} = \frac{\displaystyle\int_0^{2\pi}-\frac{\partial T}{\partial y}\bigg|_{y=0}\mathrm{d}x}{\displaystyle\int_0^{2\pi}\frac{\mathrm{d}x}{1+\epsilon\cos x}} \tag{3.48}$$

$$= Q_1 + Pe^{-\frac{1}{2}}Q_2 + O(Pe^{-1}), \tag{3.49a}$$

with

$$Q_1 = \frac{(1-\epsilon^2)^{\frac{1}{2}}}{2\pi}\int_0^{2\pi}\frac{1-T_{\text{i}}}{y_+(x)}\mathrm{d}x, \tag{3.49b}$$

$$Q_2 = \frac{(1-\epsilon^2)^{\frac{1}{2}}}{2\pi}\int_0^{2\pi}\frac{T_{\frac{1}{2}}(\sigma=0)}{y_+(x)}\mathrm{d}x. \tag{3.49c}$$

Using $\bar{\psi}$ of (2.13), valid to $O(\epsilon)$, the radial locations of the hyperbolic stagnation point A, y_A, and that of Γ_+, y_+, are all obtained numerically. These are inserted into (3.45)

and (3.46) to solve for $T_{\frac{1}{2}}(\sigma = 0)$ and Q_1 and Q_2 to obtain the steady enhancement $\bar{D}_{\text{eff}}/D$. While the solution (3.49) is more involved, its estimates of the enhancement is in excellent agreement with the numerical value as evident in figure 4.

4. Analysis of the periodically forced system and time-averaged enhancement

An oscillating rotation speed of the outer cylinder introduces a time-periodic perturbation which gives rise to chaotic particle paths (Aref 1983, 1984). A particular Poincaré section of the flow is the time-T map, Σ^T, with $T = 2\pi/\omega$ which is the time-period of the periodic perturbation. For the steady flow, $\alpha = 0$, a time-T map is then snapshots of tracer particles travelling along streamlines and would reproduce figure 2. In figure 5 we show a Poincaré section of the perturbed flow at large time which has been perturbed with a forcing amplitude of $\alpha = 0.5$. All Poincaré sections are obtained using the flow field in bipolar coordinates. The chaotic dynamics evident in the figure has the characteristics of Hamiltonian chaos like homoclinic tangles and Cantori etc. Since these have been mostly well studied and documented for such systems as ours (Aref & Balachandar 1986; Solomon & Gollub 1988; Rom-Kedar *et al.* 1990), we shall not reproduce them here. It is also evident from figure 5 that, in certain distinct regions of the flow domain, the time-T map has no smooth invariant curves or manifolds unlike that in the steady case and fluid elements wander across the separatrix Γ in a random fashion. Nevertheless, this chaotic or seemingly random motion is bounded within a stochastic layer for small α. Outside the stochastic layer, particle paths in Ω_1 and Ω_2 may still trace out closed, near-concentric circles even though there is a periodic azimuthal variation. Within Ω_1, the family of closed streamlines around the elliptic point B are also perturbed producing a series of thin chaotic layers, bounded by impenetrable Kolmogorov, Arnold & Moser (KAM) curves which are invariant curves of the time-T map. As the amplitude of the perturbation is increased, there are fewer regular domains and the stochasticity becomes more widespread owing to the disintegration of KAM curves. The analysis of §3 shows that, at the high Pe limit, the steady flow field effectively expels any temperature (or concentration) gradient within Ω_i at steady state. Thus, in the unsteady flow, chaotic layers within Ω_i will not contribute significantly to the time-averaged transport enhancement in this limit of Pe after the initial transient. Consequently, we shall focus on the chaotic layer in the vicinity of the separatrix Γ, which we refer to as the stochastic layer without fear of ambiguity to estimate transport enhancement due to chaotic mixing.

The physical mechanism underlying chaotic transport enhancement is quite evident from figure 5. In the steady problem of the previous section, it is clear that the major resistance to steady transport occurs at the diffusively dominant outer regions Ω_1 and Ω_2 and at the boundary layer near the separatrix. In contrast, there is negligible resistance within the recirculation region Ω_1 because of the mixing effect of recirculation. The stochastic layers near the separatrices in figure 5 then cause additional mixing in the critical areas by introducing stochastic particle motion. They allow fluid elements to cross the bounding separatrices and increase the local diffusion rate in the regions where they invade into Ω_1 and Ω_2. Hence, to estimate chaotic transport enhancement, we shall need to obtain the width of the stochastic layers and the effective diffusion rate within the layers. Moreover, since the effect of chaotic enhancement is not important deep in Ω_1 at high Pe because of the dominance of advection mixing there, the major contribution of chaotic mixing

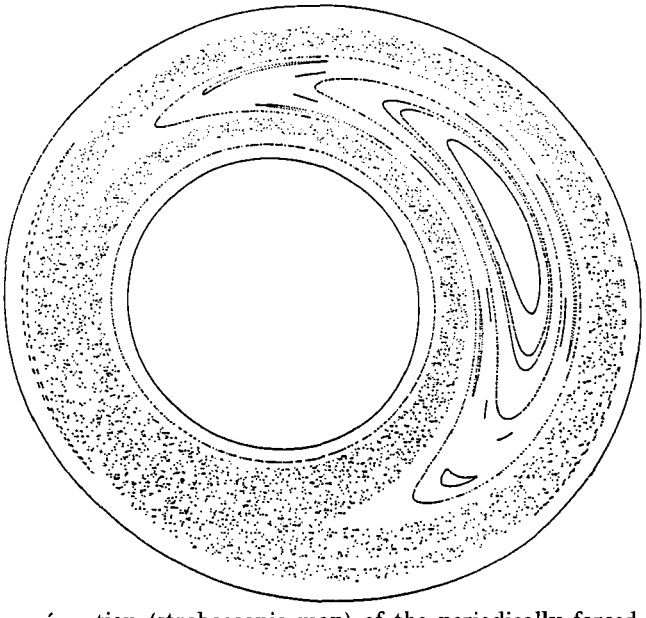

FIGURE 5. A Poincaré section (stroboscopic map) of the periodically forced system where the particle locations from a series of initial conditions are recorded after a period equal to the period of the forcing function. Notice that the stochastic layer around Γ is bounded since a closed streamline around the inner cylinder is still evident in Ω_2. Notice also the stochastic layers around the KAM islands within Ω_1. Parameter values are $\alpha = 0.5$, $\epsilon = 0.2$, $\delta = 1.0$ and $\omega = 0.3$.

occurs near the separatrix at high *Pe*. Hence, the enhancement by wide stochastic layers under large-amplitude forcing is expected to be well approximated by a thin-layer theory for weak forcing. We shall show that both the width and the effective diffusion within the stochastic layers can be obtained analytically by studying the trajectories near the separatrices under the influence of weak periodic forcing. Our theory involves the local construction of a map near the separatrix and the relative insignificance of the particle motion away from the separatrix allows us to use this local map in spite of its inaccuracy after a large number of iterations when the trajectory has moved far away (Rom-Kedar 1990). We then combine the result with the steady enhancement of the previous section to yield an overall time-averaged enhancement rate. A surprising result of our analysis is that we can then optimize the forcing frequency to maximize chaotic enhancement, a task that seems exceedingly difficult at first glance because of the complexity of the process. That a finite optimal frequency exists is also surprising and this is important in future practical application of chaotic transport enhancement. Consistent with the above speculation, we show that our prediction of the optimum frequency from a weak forcing theory remains valid at strong forcing. Our analysis also reveals how the enhancement varies as a function of forcing amplitude.

4.1. *Construction of separatrix and standard maps near the separatrices*

For small amplitudes of perturbation, $\alpha \ll 1.0$, the behaviour of the trajectories near the separatrices under the influence of periodic forcing can be estimated from a separatrix map or whisper map (Chirikov 1979; Weiss & Knobloch 1989) which reduces to the standard map for forced oscillators. The separatrix map is used to examine the dynamics of particle motion in the outer neighbourhood of Γ. The map

is constructed by considering the change in the stream function ψ over successive crossings of a surface fixed in the physical space. The surface Σ is placed along a radial line of $x = 0$ and the separatrix map is therefore a Poincaré map for the stream function ψ of a particle trajectory near Γ as it interests the $x = 0$ radial position at every circuit. For the steady flow field ($\alpha = 0$), this Poincaré map is just trivially the identity map. At $\alpha \neq 0$, it can be seen from (2.12), that the time dependence in $\psi(x, y, t)$ is entirely contained in $\alpha\hat{\psi}(x, y, t)$. Since $\alpha\hat{\psi}(x, y, t)$ is periodic both in x and t, its variation is bounded and small for $\alpha \ll 1.0$. Hence, following Chirikov (1979), we compute changes in only the leading-order aperiodic steady part of ψ, $\bar{\psi}(x, y)$, after each circuit. If the value of $\bar{\psi}(x, y)$ is $\bar{\psi}^n$ at the nth crossing of the surface Σ, its value at the next intersection is given by

$$\bar{\psi}^{n+1} = \bar{\psi}^n + \int_\Gamma \frac{\mathrm{d}\bar{\psi}}{\mathrm{d}t}\,\mathrm{d}t, \tag{4.1}$$

where the $\bar{\psi}$ value is understood to be at $x = 0$ and the integration is along the branch Γ of the unperturbed double homoclinic loop, which is an approximation valid only in the neighbourhood of Γ. Since the double homoclinic loop has two branches, Γ_+ and Γ_-, the surface of section map of (4.1) will depend on the particular branch in consideration and Γ can denote either the outer branch Γ_+ or the inner branch Γ_-. Clearly (4.1) will not be valid for orbits within Ω_1, since they alternate from the vicinity of Γ_+ to the vicinity of Γ_- and the integration cannot be carried out along a specific branch of Γ. Fortunately, as stated earlier, only the outer neighbourhood of Γ is pertinent since the inner side within Ω_1 is already gradientless owing to high Pe steady enhancement. Inserting (2.13) and (2.14) into (4.1), one obtains

$$\bar{\psi}^{n+1} = \bar{\psi}^n - \alpha M_\Gamma(t_0^n), \tag{4.2}$$

$$M_\Gamma(t_0) = \int_{-\infty}^{+\infty} \left(-\frac{\partial\bar{\psi}}{\partial y}, \frac{\partial\bar{\psi}}{\partial x}\right)(x_s(t), y_s(t)) \Lambda \left(-\frac{\partial\hat{\psi}}{\partial y}, \frac{\partial\hat{\psi}}{\partial x}\right)(x_s(t), y_s(t), t + t_0)\,\mathrm{d}t$$

$$= \int_{-\infty}^{+\infty} (\bar{u}, \bar{v})\,(x_s(t), y_s(t))\,\Lambda(\hat{u}, \hat{v})\,(x_s(t), y_s(t)) \sin\omega(t + t_0)\,\mathrm{d}t. \tag{4.3}$$

The wedge product is defined by $(f_1, f_2)\,\Lambda(g_1, g_2) = f_1 g_2 - f_2 g_1$ and is evaluated along $(x_s(t), y_s(t))$ which represents the trajectory $\Gamma(t)$ in the steady flow. Note that M_Γ is different for each branch of the homoclinic loop. The variable t_0 is to account for the phase difference between the unperturbed trajectory and the perturbation. It lies in the range $[0, T]$, $T = 2\pi/\omega$. A convenient scaling

$$\tau_0 = \omega t_0 \tag{4.4}$$

then confines the phase τ_0 to the interval $[0, 2\pi]$. From (4.2), the change in $\bar{\psi}(x, y)$ over successive crossings of the surface of section Σ depends on the value of the phase τ_0 at Σ. We therefore construct a mapping for the phase τ_0. Since τ_0^{n+1} is the phase difference at the $(n+1)$th circuit it is related to τ_0^n by the circuit time of the $(n+1)$th circuit,

$$\tau_0^{n+1} = \tau_0^n + \omega P(\bar{\psi}^{n+1}), \tag{4.5}$$

where $P(\bar{\psi})$ is the circuit time of a unperturbed trajectory with streamfunction $\bar{\psi}$, in the outer neighbourhood of Γ. The separatrix map is then the two dimensional map

$$\bar{\psi}^{n+1} = \bar{\psi}^n - \alpha M_\Gamma(\tau_0^n), \tag{4.6}$$

$$\tau_0^{n+1} = \tau_0^n + \omega P(\bar{\psi}^{n+1}). \tag{4.7}$$

The map of (4.6) and (4.7) applies only in the neighbourhood of Γ exterior to the recirculation region Ω_1 where Γ can be Γ_+ or Γ_- and each case will be considered separately but will be shown to be identical to leading order in ϵ.

It is easily shown that the Melnikov function, $M_\Gamma(\tau_0)$, is a periodic function of the form,

$$M_\Gamma(\tau_0) = A_\Gamma(\epsilon, \delta, \omega) \sin(\tau_0 + \phi_\Gamma(\epsilon, \delta, \omega)). \tag{4.8}$$

The Melnikov function corresponding to either branch of the double homoclinic loop must then cross zero for some $\tau_0 \in [0, 2\pi]$ and $M_\Gamma(\tau_0)$ of (4.8) has at least two zeros. From the Melnikov theory, this confirms the existence of chaotic particle paths in the time-periodic flow since a zero of the Melnikov function implies the intersection of stable and unstable manifolds (homoclinic tangles) associated with the hyperbolic saddle point of the time-T Poincaré map and, thus, the existence of a Smale horseshoe with stretching and folding operations (theorems 4.5.3 and 5.3.5 of Guckenheimer & Holmes 1983). We shall use the flow field in local Cartesian coordinates, u and v of (2.10) and (2.11), to express the Melnikov function of (4.3) in the form of (4.8) and obtain an analytical expression for A_Γ and ϕ_Γ to leading order in ϵ. For simplicity, we shall consider only Γ_+.

Thus, from (4.3),

$$M_{\Gamma_+}(\tau_0) = B^1_{\Gamma_+}(\epsilon, \delta, \omega) \cos(\tau_0) + B^2_{\Gamma_+}(\epsilon, \delta, \omega) \sin(\tau_0), \tag{4.9}$$

with

$$B^1_{\Gamma_+}(\epsilon, \delta, \omega) = \int_{-\infty}^{+\infty} [\bar{u}(x_+(t), y_+(t))\, \hat{v}(x_+(t), y_+(t)) - \bar{v}(x_+(t), y_+(t))\, \hat{u}(x_+(t), y_+(t))] \sin \omega t \, \mathrm{d}t, \tag{4.10}$$

$$B^2_{\Gamma_+}(\epsilon, \delta, \omega) = \int_{-\infty}^{+\infty} [\bar{u}(x_+(t), y_+(t))\, \hat{v}(x_+(t), y_+(t)) - \bar{v}(x_+(t), y_+(t))\, \hat{u}(x_+(t), y_+(t))] \cos \omega t \, \mathrm{d}t, \tag{4.11}$$

where $(x_+(t), y_+(t))$ represents trajectory $\Gamma_+(t)$ in the steady flow. equation (4.9) can now be expressed in the form (4.8) with

$$A_{\Gamma_+}(\epsilon, \delta, \omega) = \left(B^2_{1\Gamma_+} + B^2_{2\Gamma_+}\right)^{\frac{1}{2}}, \tag{4.12}$$

$$\phi_{\Gamma_+}(\epsilon, \delta, \omega) = \tan^{-1}\left(\frac{B^1_{\Gamma_+}}{B^2_{\Gamma_+}}\right). \tag{4.13}$$

To obtain $B^1_{\Gamma_+}$ and $B^2_{\Gamma_+}$, we shall convert the time integrations of (4.10) and (4.11) into an integration over the azimuthal direction x. In the steady flow, $\mathrm{d}x/\mathrm{d}t = \bar{u}(x, y)$, where $\bar{u}$ is obtained from (2.10). Since $y = y_+(x)$ on Γ_+, with $y_+(x)$ given by (3.21), one obtains to leading order in ϵ

$$\mathrm{d}t = \frac{-\epsilon^{-\frac{1}{2}} \mathrm{d}x}{(1+\delta)\, y_\Gamma(x)}, \tag{4.14}$$

$$t(x) = -\epsilon^{-\frac{1}{2}} \frac{(1+\delta)}{\sqrt{2\delta}} \ln|\tan(\tfrac{1}{4}x + \tfrac{1}{4}\pi)|, \tag{4.15}$$

where $t(x)$ gives time as a function of azimuthal position on Γ_+ with initial time $t = 0$ at $x = 0$. As expected, $t(x)$ goes from $+\infty$ to $-\infty$ as x goes from $-\pi$ to $+\pi$. Since $\bar{u}$, $\bar{v}$, $\hat{u}$, $\hat{v}$ in (4.10) and (4.11) are also evaluated along Γ_+, we replace $x_+(t)$ by x and

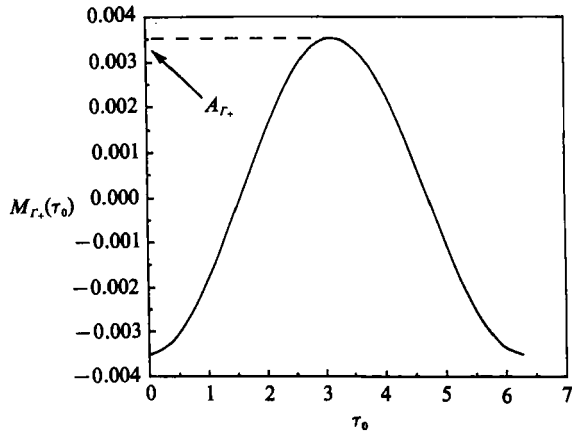

FIGURE 6. Leading-order estimate of the Melnikov function at the outer separatrix Γ_+ as a function of the τ_0. Two zeros are clearly evident, indicating the existence of homoclinic tangle. Parameter values are $\epsilon = 0.2$ and $\delta = 1.0$.

the velocity components are now evaluated at $(x, y_+(x))$. Thus, inserting $y_+(x)$ of (3.21) in $\bar{u}$, $\bar{v}$, $\hat{u}$ and $\hat{v}$ and using (4.13) and (4.14), (4.10) and (4.11) are expanded to leading order in ϵ to yield

$$B^1_{\Gamma_+} = \frac{\epsilon^{\frac{1}{2}}\delta^2}{(1+\delta)^3}\int_{-\pi}^{+\pi} \frac{\sin x}{(1+\cos x)^{\frac{1}{2}}} \sin\left\{\omega\left[-\epsilon^{-\frac{1}{2}}\frac{(1+\delta)}{\sqrt{2\delta}}\ln|\tan(\tfrac{1}{4}x+\tfrac{1}{4}\pi)|\right]\right\} \mathrm{d}x, \quad (4.16)$$

$$B^2_{\Gamma_+} = \frac{\epsilon^{\frac{1}{2}}\delta^2}{(1+\delta)^3}\int_{-\pi}^{+\pi} \frac{\sin x}{(1+\cos x)^{\frac{1}{2}}} \cos\left\{\omega\left[-\epsilon^{-\frac{1}{2}}\frac{(1+\delta)}{\sqrt{2\delta}}\ln|\tan(\tfrac{1}{4}x+\tfrac{1}{4}\pi)|\right]\right\} \mathrm{d}x. \quad (4.17)$$

A_{Γ_+} and ϕ_{Γ_+} are then evaluated using (4.12) and (4.13) respectively. The Melnikov function, $M_{\Gamma_+}(\tau_0)$, is plotted against τ_0 in figure 6 for a pair of A_{Γ_+} and ϕ_{Γ_+} obtained from the leading-order analytical estimates outlined above. Two zeros are clearly evident confirming the existence of chaotic transport. For Γ_-, we use $y_-(x)$ of (3.21), and following the same procedure as outlined for Γ_+, it is easily shown that to leading order in ϵ,

$$A_{\Gamma_-} = A_{\Gamma_+}, \quad (4.18)$$

$$\phi_{\Gamma_-} = \phi_{\Gamma_+}, \quad (4.19)$$

and we shall refer to them collectively as A_Γ and ϕ_Γ. It is found that A_Γ is non-zero and finite for all non-zeros values of ϵ, δ and ω. Thus for any finite amplitude of the periodic forcing, chaotic particle paths exist for the entire parametric range over which the analysis is valid. We emphasize that the theory is valid only for small α. While the existence of zeros of the Melnikov functions shown in figure 6, confirms the existence of chaotic motions, it does not indicate how widespread the chaotic particle motion is. We shall address this through the separatrix map of (4.6) and (4.7).

The separatrix map is still too complicated to allow any analysis. Since $\alpha \ll 1.0$, variations in $\bar{\psi}$ over successive iterations of the map are small provided A_Γ is small, and we can linearize the map in $\bar{\psi}_{n+1}$ about a trajectory in the outer neighbourhood of Γ. Defining the normalized deviation stream function

$$w^n = \frac{(\bar{\psi}_\Gamma - \bar{\psi}^n)}{\bar{\psi}_\Gamma}, \quad (4.20)$$

where $\bar{\psi}_\Gamma$ is the value of $\bar{\psi}$ on Γ and is, hence, the value of $\bar{\psi}$ at (π, y_A) i.e. $\bar{\psi}_\Gamma = \bar{\psi}(\pi, y_A)$. Since the validity of the separatrix map is restricted to the outer neighbourhood of Γ, $\bar{\psi}^n < \bar{\psi}_\Gamma$ and w is a positive quantity. Then, linearizing (4.7) about a characteristic orbit, w^*,

$$\begin{aligned} \tau_0^{n+1} &= \tau_0^n + \omega P(w^{n+1}) \\ &\simeq \tau_0^n + \omega[P(w^*) + P'(w^{n+1} - w^*)] \end{aligned} \tag{4.21}$$

in terms of the normalized deviation stream function w, (4.6) becomes

$$w^{n+1} = w^n + \left(\frac{\alpha A_\Gamma}{\bar{\psi}_\Gamma}\right) \sin(\tau_0^n + \phi_\Gamma(\epsilon, \delta, \omega)). \tag{4.22}$$

Thus, the linearization is valid only if

$$\alpha A_\Gamma \ll 1. \tag{4.23}$$

Since $\bar{\psi}_\Gamma \sim \delta^2/2(1+\delta)$ is of order unity. We shall choose w^* to correspond to a resonant orbit with circuit time an integral multiple of the forcing period, T.

$$P(w^*) = mT = m\frac{2\pi}{\omega}, \tag{4.24}$$

where m is an integer. Hence, (4.17) becomes

$$\tau_0^{n+1} = \tau_0^n + 2m\pi + \omega P'(w^*)(w^{n+1} - w^*). \tag{4.25}$$

Since $\tau_0^n - 2m\pi = \tau_0^n$ by definition, the phase map is further simplified by eliminating $2m\pi$ from (4.25). To convert to the conventional action-angle coordinates, we define

$$I^{n+1} = \omega P'(w^*)(w^{n+1} - w^*), \tag{4.26}$$

$$\theta^n = \tau_0^n + \phi_\Gamma, \tag{4.27}$$

and the standard map (Chirikov 1979) results in

$$I^{n+1} = I^n + K_\Gamma \sin\theta^n, \tag{4.28}$$

$$\theta^{n+1} = \theta^n + I^{n+1}, \tag{4.29}$$

where the 'stochasticity parameter' K_Γ corresponding to a given branch of the double homoclinic loop is

$$K_\Gamma = \frac{\alpha\omega P'(w^*) A_\Gamma}{A_\Gamma}. \tag{4.30}$$

We note that K_Γ is dependent on the normalized stream function w^* for the resonant orbit.

4.2. *Estimates of the width and effective diffusivity of the stochastic layers*

The standard map of (4.28) and (4.29) has been studied extensively in the literature (see Lichtenberg & Lieberman, 1983, and references therein) and it has been shown that for $|K_\Gamma|$ greater than a critical value, K_c, called the stability border of K_Γ, variations in I become chaotic. Thus chaotic motions occur for the standard map when

$$|K_\Gamma| > K_c = 0.972. \tag{4.31}$$

Since the resonant orbits of the separatrix map, w^*, are dense close to Γ, $P'(w^*)$ can be replaced by $P'(w)$. The quantity $P(w)$ is singular at the separatrix and it decreases

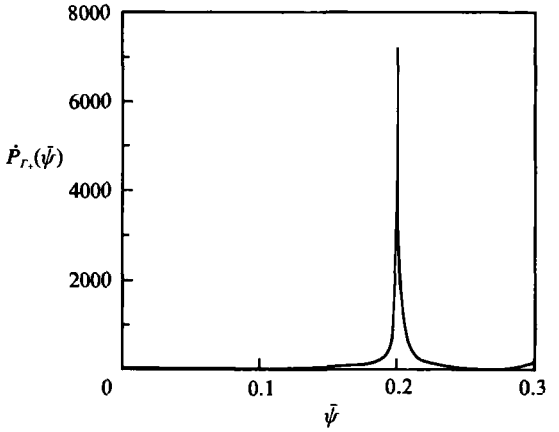

FIGURE 7. Computed rate of change of the circuit time away from the separatrix Γ_+ as a function of the steady stream function. The estimate of (4.39) lies on top of the computed value with $\bar{\psi}_\Gamma = 0.2$ and is not drawn. Parameter values are $\epsilon = 0.2$ and $\delta = 1.0$.

rapidly as one moves away from away from Γ. Thus, $P'(w)$ also decreases monotonically with increasing w as one moves into Ω_1 and Ω_2 (see figure 7). Consequently, one expects chaotic trajectories in the outer neighbourhood of Γ up to a distance determined by

$$K_\Gamma(w_c) = K_c. \tag{4.32}$$

The stochastic layer is then confined within $w \leqslant w_c$. In terms of the steady stream function, $\bar{\psi}$, the stochastic layer outside Γ is confined within

$$\bar{\psi}_c \leqslant \bar{\psi} \leqslant \bar{\psi}_\Gamma \tag{4.33}$$

where $\bar{\psi}_c$ is given by the relationship

$$\dot{P}(\bar{\psi}_c) = \frac{K_c}{\alpha\omega A_\Gamma(\epsilon, \delta, \omega)}, \tag{4.34}$$

where the dot now denotes derivative with respect to $\bar{\psi}$ instead of w and the width $L_{\bar{\psi}}$ of the stochastic layer, external to Γ, is given in terms of the steady stream function

$$L_{\bar{\psi}} = \bar{\psi}_\Gamma - \bar{\psi}_c \tag{4.35}$$

and holds at every azimuthal position x. This can be converted into actual width L by using the local expansion on the surface Σ at $x = 0$,

$$\Delta\bar{\psi} = \left(\frac{\partial\bar{\psi}}{\partial y}\right)(x = 0,\ y = y_\pm(0))\,\Delta y \sim \frac{2\epsilon^{\frac{1}{2}}\delta}{(1+\delta)}\Delta y, \tag{4.36}$$

such that the width of the stochastic layer is estimated to be

$$L \sim L_{\bar{\psi}}(1+\delta)/(2\epsilon^{\frac{1}{2}}\delta). \tag{4.37}$$

Further simplification can be made if the circuit time $P(\bar{\psi})$ can be estimated. This is achieved by using the leading-order estimate of the steady flow field in (2.13*b*). To zeroth order in the eccentricity ϵ, the circuit time is obtained by integrating (2.15) around the gap to yield

$$P \sim \frac{2\pi}{(1+\delta)|\bar{\psi} - \bar{\psi}_*|} \sim \frac{2\pi}{(1+\delta)|\bar{\psi} - \bar{\psi}_\Gamma|} + O(\epsilon), \tag{4.38}$$

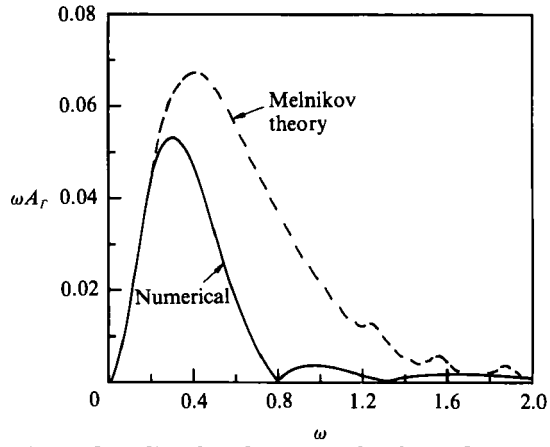

FIGURE 8. Comparison of predicted and computed values of ωA_Γ at $\Gamma_+(\epsilon = 0.2$ and $\delta = 1.0)$.

and using (4.20) to link w and $\bar{\psi}$, one obtains

$$\dot{P} = \frac{\mathrm{d}P}{\mathrm{d}\bar{\psi}} \sim \frac{2\pi}{(1+\delta)|\bar{\psi} - \bar{\psi}_\Gamma|^2}. \tag{4.39}$$

This estimate is in excellent agreement with the computed values in figure 7 and is not drawn. Equations (4.29) and (4.34) then allow a simple explicit expression for both L_ψ and L,

$$|\bar{\psi}_c - \bar{\psi}_\Gamma| = L_\psi = \left[\frac{2\pi\alpha\omega A_\Gamma(\epsilon, \delta, \omega)}{(1+\delta)K_c}\right]^{\frac{1}{2}}, \tag{4.40}$$

and L is still given by (4.37). It is then evident that L varies as $\alpha^{\frac{1}{2}}$ and increasing the forcing amplitude should effect a monotonic increase in the enhancement. The variation with the forcing frequency ω is more complex. We note that this ω-dependence is contained in $\omega A_\Gamma(\epsilon, \delta, \omega)$ and large ωA_Γ would imply large L. The expressions (4.12), (4.16) and (4.17), are used to obtain the ωA_Γ values in figure 8 at different ω and at $\epsilon = 0.2$ and $\delta = 1.0$. The exact values from (4.3) are also computed with the flow field of (2.10) and (2.11). Comparison to our estimate in figure 8 shows good agreement. Multiple but successively diminishing maxima are observed. The smaller maxima are not well resolved by our analysis and this is attributed to higher-order effects of ϵ, not incorporated in (4.16) and (4.17). There appears to be an optimum forcing frequency, $\omega_c \simeq 0.4$, where the stochastic layer is thickest with fast decay on either side. This prediction is verified numerically as shown in figure 9 where Poincaré sections of a tracer particle initially located near the hyperbolic saddle point A are depicted. It is clearly evident that the stochastic layer is of largest width L at the optimum forcing frequency $\omega_c \approx 0.4$. The estimate of L at this frequency can be extracted from (4.37) and (4.40). From figure 8, ωA_Γ is predicted to be approximately 0.07 at ω_c which yields $L_\psi = 0.21$ and $L = 0.47$. This is of the same magnitude as the azimuthally averaged thickness in figure 9(*b*) even though our estimate should not be accurate for such a thick layer.

For $K_\Gamma \gg K_c$ (i.e. close to the separatrix), the stochastic variations in the action I of the standard map of (4.28) and (4.29) can be approximated by a diffusion process in I (Chirikov 1979). It should be noted that Karney (1983) has shown that this diffusion is only valid at extremely large K_Γ when the 'stochastic sea' engulfs the entire phase space. At lower values of K_Γ, surviving islands appear within the sea

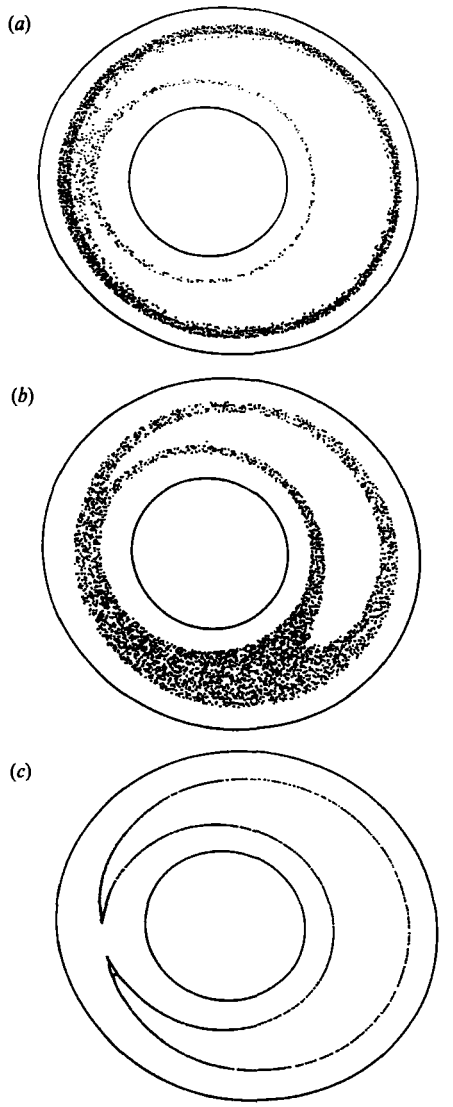

FIGURE 9. Poincaré section of the stochastic layer in the vicinity of Γ at (*a*) $\omega = 0.01$, (*b*) $\omega = 0.4$ and (*c*) $\omega = 0.7$ showing a clear maximum at $\omega_c = 0.4$ ($\epsilon = 0.2$, $\delta = 1.0$ and $\alpha = 0.2$).

which destroy the stochastic nature of particle motion and give rise to anomalous diffusion. The high K_Γ limit corresponds to the region next to the separatrix where K_Γ approaches infinity from (4.30) and (4.39). In this limit, one can invoke the ergodic assumption and it can be easily shown from a phase-space average of (4.30) that the first moment of the variation in action I is zero while the second moment grows linearly with n,

$$\langle \Delta I \rangle = 0, \tag{4.41}$$

$$\langle \Delta I^2 \rangle = \tfrac{1}{2} n K_\Gamma^2, \tag{4.42}$$

where the angle brackets denote expectation. Hence, from the definition of Markov diffusion processes, the variations in action I is a diffusion-like process in this limit with a zero drift coefficient and a diffusivity of $\frac{1}{4}K_\Gamma^2$,

$$D_I^{\text{map}} = \tfrac{1}{4} K_\Gamma^2. \tag{4.43}$$

The diffusivity of the flow field is then obtained using the following relation between maps and flows

$$D^{\text{map}} = \bar{P} D^{\text{flow}}, \tag{4.44}$$

where $\bar{P}$ is the mean time between successive iterations of the map. At the separatrix, P approaches infinity and it decays by $|\bar{\psi} - \bar{\psi}_\Gamma|^{-1}$ away from the separatrix as indicated by (4.38). Hence, we aim to obtain an upper bound on the effective diffusivity and choose $\bar{P}$ to be the value $P(\bar{\psi}_c)$ where D^{flow} is largest. This quantity can be easily estimated from (4.38) and (4.40). An average $P(\bar{\psi})$ over the entire stochastic layer is not possible owing to the $|\bar{\psi} - \bar{\psi}_\Gamma|^{-1}$ singularity at the separatrix. Thus, the effective diffusivity in I owing to the chaotic transport within the stochastic layer is bounded by

$$D_I = \frac{1}{4} \frac{K_\Gamma^2}{P(\bar{\psi}_c)}, \tag{4.45}$$

where $\bar{\tau}$ is the mean time between successive intersections of a trajectory with the surface.

While (4.45) is strictly valid only at $K_\Gamma \gg K_c$, we shall assume that it holds over the entire width L_Γ, in keeping with our estimate of an upper bound to time-averaged enhancement. Since stochastic variations in I imply stochastic variations in $\bar{\psi}$, one obtains from (4.26)

$$\begin{aligned} \langle \Delta I^2 \rangle &= [\omega P'(w)]^2 \langle \Delta w^2 \rangle \\ &= [\omega \dot{P}(\bar{\psi})]^2 \langle \Delta \bar{\psi}^2 \rangle. \end{aligned} \tag{4.46}$$

Hence, the diffusion in $\bar{\psi}$ is simply

$$\begin{aligned} D_{\bar{\psi}} &= K_\Gamma^2 / \{4\Pi(\bar{\psi}_c)\,[\omega \dot{P}(\bar{\psi})]^2\} \\ &= \frac{\alpha^2 A_\Gamma^2}{4P(\bar{\psi}_c)}, \end{aligned} \tag{4.47}$$

after substituting (4.30). This can be converted to diffusivity in the local radial coordinate by using (4.36),

$$\begin{aligned} D_s &\sim D_{\bar{\psi}} \left(\frac{\partial \bar{\psi}}{\partial y} \right)^2 \\ &\sim \frac{\alpha^2 A_\Gamma^2 (1+\delta)^2}{16 \epsilon \delta^2 P(\bar{\psi}_c)}. \end{aligned} \tag{4.48}$$

This estimate of the effective diffusivity due to stochastic transport can be further simplified by using the estimates for $P(\bar{\psi}_c)$ and $L_{\bar{\psi}}$ in (4.38) and (4.40),

$$D_s \sim \left(\frac{2w}{\pi K_c} \right)^{\frac{1}{2}} \frac{[\alpha A_\Gamma (1+\delta)]^{\frac{5}{2}}}{32 \epsilon \delta^2}. \tag{4.49}$$

This represents the most convenient upper bound on the effective radial diffusivity of the stochastic transport across the separatrices Γ owing to homoclinic entanglement. Because of the symmetries of (4.18), the diffusivities at the two separatrices Γ_+ and Γ_- are identical to leading order. Since A_Γ is a complex function of ω, ϵ and δ. The effects of these parameters on D_s are not explicit and must be numerically derived from the Melnikov result of (4.12). In fact, the non-monotonic behaviour with respect to ω is already apparent in figure 8. The maximum of L with respect to ω coincides with the maximum of ωA_Γ at ω_c by virtue of (4.40). (The optimal frequency for maximum width occurs at $\omega_c \sim 0.4$ for the conditions in figure 8.) However, owing to an additional factor of ω^2 in (4.49), the maximum in the effective diffusivity is expected to shift slightly from ω_c. The shift is small, however, because of the small magnitude of ωA_Γ relative to ω near ω_c. Hence, we expect a

maximum time-averaged enhancement to occur for a forcing frequency near ω_c. This will be verified in the subsequent analysis. The effect of α is more explicit. Since the width of the stochastic layer L increases as $\alpha^{\frac{1}{3}}$ and D_s by $\alpha^{\frac{5}{3}}$, we hence expect a monotonic increase in time-averaged enhancement with respect to forcing amplitude. Finally, it should be noted that, owing to the constraint (4.23), our Melnikov analysis is strictly valid for thin layers with small diffusivities. This is not to say that thick layers with large diffusivities cannot be introduced with periodic perturbation. It simply needs to be studied numerically.

4.3. *Derivation of time-averaged enhancement*

We shall now utilize our estimated time-averaged diffusivity of stochastic transport in (4.49) to obtain an estimate of the time-averaged diffusivity. Since D_s is small, we assume that the ratio of stochastic to molecular diffusivities $D_s Pe$ is of order unity. Since the chaotic transport is statistically independent of molecular diffusion, the sum of two independent Markov diffusion processes, each with zero drift and finite diffusion coefficient, is also a Markov diffusion process with zero drift and the diffusion coefficient is equal to the sum of the two independent processes. Hence, the effective normalized time-averaged diffusivity within the stochastic layer is $1+D_s Pe$ and a simple flux balance yields the time-averaged flux at the Γ_+ boundary of the stochastic layer.

$$\frac{\partial T}{\partial y}(y_+(x)) = [T(y_+)-1]\frac{(1+PeD_s)}{(y_+-L)\left[(1+PeD_s)+\dfrac{L}{y_+-L}\right]}. \tag{4.50}$$

If PeD_s is negligible, this reduces to condition (3.34*b*) of the unperturbed system, after transformation to the σ coordinate of the diffusive boundary as expected. If PeD_s approaches infinity, corresponding to a small stochastic diffusivity that is nevertheless much greater than molecular diffusivity Pe^{-1}, (4.50) reduces to

$$\frac{\partial T}{\partial y}(y_+(x)) = \frac{[T(y_+)-1]}{y_+-L}. \tag{4.51}$$

This reflects the physical picture that, since stochastic diffusivity is much in excess of its molecular counterpart, the time-averaged temperature field within the stochastic layer is also uniform as in the recirculation region. This essentially enlarges the recirculation by a width of L on both sides. Hence, the width of the diffusive region Ω_1 is reduced from y_+ to y_+-L. This accounts for the difference between (4.51) and (3.34*b*).

Using (4.50) in place of (3.34*b*), our estimate of the time-averaged enhancement then proceeds as the steady enhancement of §3. We use the expansion

$$\frac{1}{y_+-L} \sim \frac{1}{y_s}\left(1+\frac{\epsilon^{\frac{1}{3}}y_\Gamma+L}{y_s}\right) \tag{4.52}$$

as before but now stipulating that L, which must be small for our Melnikov analysis to be valid, is of $O(\epsilon^{\frac{1}{3}})$. It can then be readily shown that the time-averaged enhancement is related to the steady enhancement by

$$\frac{\langle \bar{D}_{\text{eff}}\rangle}{D} = \frac{\bar{D}_{\text{eff}}}{D}+\frac{L}{y_s}\left(\frac{PeD_s}{1+PeD_s}\right) \tag{4.53}$$

$$= \frac{\bar{D}_{\text{eff}}}{D}+\frac{L(1+\delta)}{\delta}\left(\frac{PeD_s}{1+PeD_s}\right), \tag{4.54}$$

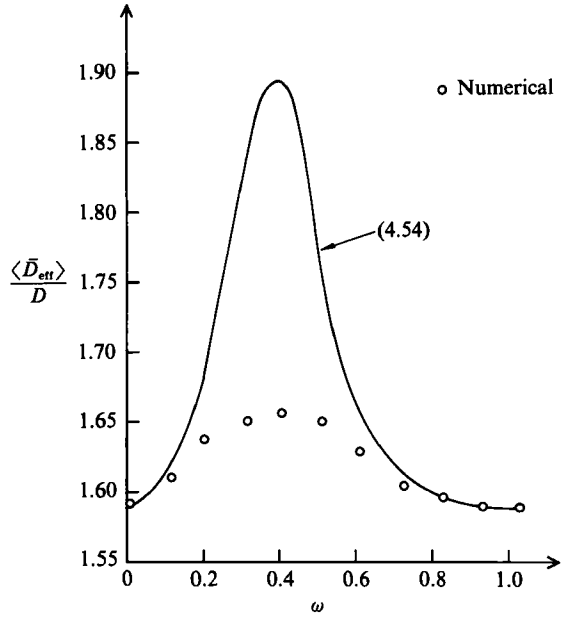

FIGURE 10. Predicted time-averaged enhancement as a function of forcing frequency compared to computed values at large time. ($Pe = 5000$, $\alpha = 0.2$, $\epsilon = 0.2$ and $\delta = 1.0$).

where the steady enhancement $\bar{D}_{\text{eff}}$ can be obtained from (3.23), (3.25), (3.42) or (3.49) and L and D_s, which result from the perturbation, are estimated from (4.37), (4.40) and (4.49). The bracket $\langle\ \rangle$ denotes time averaging here as in (3.1) instead of expectation in (4.41) and (4.42). In the limit of negligible stochastic diffusivity ($PeD_s \to 0$) or negligible width ($L \to 0$), $\langle \bar{D}_{\text{eff}} \rangle$ reduces to the steady value $\bar{D}_{\text{eff}}$. In the limit of dominant stochastic diffusivity ($PeD_s \to \infty$), (4.54) reduces to an equation that can be derived from (4.51),

$$\frac{\langle \bar{D}_{\text{eff}} \rangle}{D}(PeD_s = \infty) = \frac{\bar{D}_{\text{eff}}}{D} + \frac{L(1+\delta)}{\delta}. \tag{4.55}$$

Again, this corresponds to a simple extension of the uniform temperature region of figure 3 by a width of L on both ends of the recirculation region. It is clear that

$$\bar{D}_{\text{eff}} < \langle \bar{D}_{\text{eff}} \rangle < \langle \bar{D}_{\text{eff}} \rangle (PeD_s = \infty) \tag{4.56}$$

and (4.55) represent an even higher upper bound of the time-averaged enhancement.

In figure 10, we compare the prediction of (4.54) to computed time-averaged enhancement from a finite-difference integration of the complete time-dependent energy equation using the bipolar flow field. As is evident, the estimate is reasonably tight considering the various leading-order expansion of both the flow field and the energy equation. As expected, the estimate is good when chaotic enhancement is small and both L and D_s are accurately estimated from our local Melnikov analysis. The estimate deteriorates near $\omega_c \sim 0.4$ because of the large enhancement although ω_c is accurately predicted.

This optimum in the forcing frequency is independent of the amplitude of forcing α since A_Γ is independent of α. Thus, it is reasonable to expect the enhancement will display a maximum with respect to ω at the same ω value when the amplitude α is increased. In figure 11, numerical values of D_{eff}/D at $\alpha = 0.4$ and the same ϵ and δ

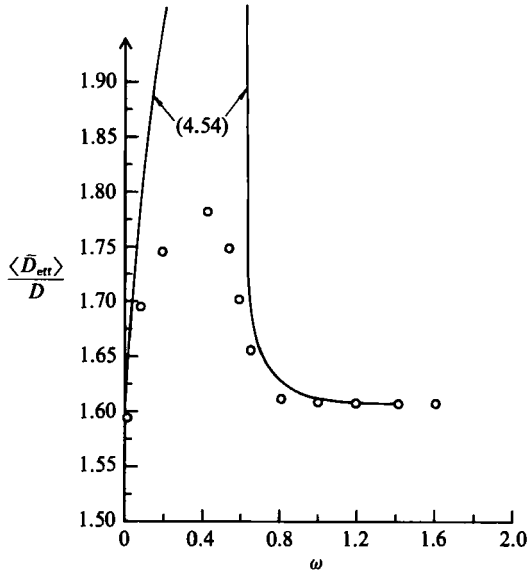

FIGURE 11. Computed and predicted time-averaged enhancement as a function of forcing frequency for $\alpha = 0.4$ and the same conditions as figure 10.

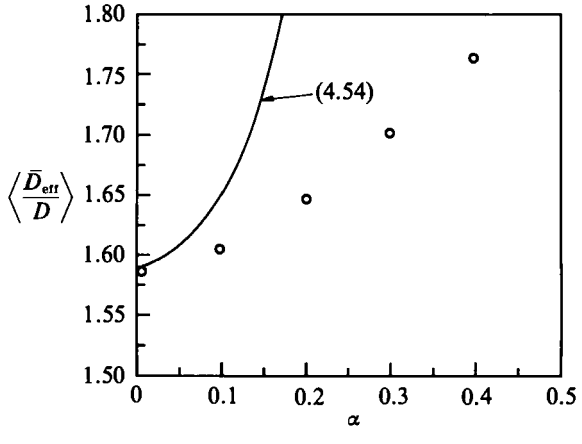

FIGURE 12. Computed and predicted time-averaged enhancement as a function of forcing amplitude at $\omega = 0.4$ and the same conditions as figure 10.

values as in figure 10 are depicted. The maximum remains even though our analysis is not expected to hold at this relatively large value of α as shown. From our analysis, it is also evident that the width L increases with increasing α. Thus, enhancement is expected to increase rapidly with increasing amplitude α and this is verified in the numerically computed values of time-averaged enhancement at several α for ω at the optimal value ω_c in figure 12. Significant enhancement as much as 50% over the steady enhancement recirculation and 100% over pure diffusion can be achieved with chaotic enhancement at large-amplitude forcing by selecting the optimum forcing frequency.

5. Summary

We have demonstrated with the eccentric cylinders as a prototype that cross-stream heat or mass transfer across a bounded nearly parallel flow can be enhanced by a slender closed recirculation region. The leading-order enhancement is independent of Pe and is of the order of the width of the recirculation region scaled by the cross-stream dimension. We have also examined the effect of perturbing the nearly parallel flow with a time-periodic forcing function such that a homoclinic entanglement of the bounding separatrices occurs which allows chaotic advection transport across the separatrices. Our Melnikov analysis shows that the penetration depth varies as $\alpha^{\frac{1}{2}}$ whereas the effective stochastic diffusivity varies as $\alpha^{\frac{1}{2}}$ where α is the forcing amplitude. An optimum forcing frequency is found which yields the largest time-averaged enhancement. Although our analysis is only valid for weak forcing and is hence only accurate for small chaotic enhancement, numerical results indicate that large enhancement over the unperturbed case can be achieved with strong forcing at the optimum frequency, which is accurately predicted by the local analysis. It should be noted that this forcing does not need to be introduced artificially. Intrinsic hydrodynamic instability can also provide the requisite perturbation. This suggests that enhancement by both the recirculation region and chaotic transport can be optimized with careful selection of system geometry and the perturbation or instability frequency. The existence of an optimum forcing frequency is most interesting. Although it is not pronounced for the present creeping flow field, one expects the power requirement to increase monotonically and rapidly with forcing frequency when hydrodynamic inertia is important. This suggests that a careful optimization can achieve maximum enhancement with minimum power input. Our analysis also explains why large heat-transfer enhancement is observed when recirculation is introduced to a nearly parallel flow. It is probable that a significant portion of the enhancement is due to chaotic transport introduced by intrinsic or external forcing. We note that this forcing does not need to be time-periodic – it can be random forcing. Nor does it need to be time-varying. A spatially-varying forcing also allows the fluid element to sample a larger portion of the cross-section surface normal to the direction in which the forcing is introduced. This is essentially the basis of a heat-exchanger tube we have designed recently to exploit heat-transfer enhancement due to chaotic mixing (Acharya *et al.* 1992). Nevertheless, it is clear from our analysis that chaotic transport can only occur if a recirculation region bounded by separatrices corresponding to homoclinic or heteroclinic loops exists. Its contribution to heat/mass transfer is only significant at high Péclet numbers and the key physical mechanism is the crossing of the bounding separatrices due to homoclinic or heteroclinic entanglement. It is fortunate that most mass transfer devices operate at high Pe and this suggests that chaotic enhancement can indeed significantly improve the performance of practical mass transfer equipment. In this respect, we observe that, although our estimates are for the prototype of eccentric cylinders, the analysis and the results can be extended in principle to other nearly parallel flows with slender recirculation. For example, in the steady estimates of (3.23), (3.25) and (3.42), the geometric parameters $\epsilon^{\frac{1}{2}}$ and δ simply correspond to the characteristic width of the slender recirculation region and the characteristic velocity jump across it. The L and D_s of the time-averaged enhancement in (4.54) can also be obtained from an appropriate Melnikov analysis of the specific stochastic layers. If the steady and perturbation flow fields are known, the analysis in the first part of §4 can be easily duplicated. Hence, analysis of other devices can easily follow

the present approach. The largest limitation of our analysis is that the Melnikov theory is only valid for small α even though figures 11 and 12 show surprising accuracy even at moderately large α. Escande & Elskens (1991) have carried out a study of the local map at large α (and small ω) which should be extendable by our formulation to analyse effective transport enhancement.

This work is supported by the Gas Research Institute under Contract no. 5090-260-1971. We thank Mr N. Acharya for help with the numerical computations.

REFERENCES

ACHARYA, N., SEN, M. & CHANG, H.-C. 1992 Heat transfer enhancement in coiled tubes by chaotic mixing. *Intl J. Heat Mass Transfer* (to appear).

AREF, H. 1983 Integrable, chaotic and turbulent vortex motion in two-dimensional flows. *Ann. Rev. Fluid Mech.* **15**, 345–389.

AREF, H. 1984 Stirring by chaotic advection. *J. Fluid Mech.* **143**, 1–21.

AREF, H. & BALACHANDAR, S. 1986 Chaotic Advection in a Stokes flow. *Phys. Fluids* **29**, 3515–3521.

BALLAL, B. Y. & RIVLIN, R. S. 1976 Flow of a Newtonian fluid between eccentric cylinders: inertial effects. *Arch. Rat. Mech. Anal.* **62**, 237–294.

BATCHELOR, G. K. 1956 On steady laminar flow with closed streamlines at large Reynolds number. *J. Fluid Mech.* **1**, 177–189.

BROOMHEAD, D. S. & RYRIE, S. C. 1988 Particle paths in wavy vortices. *Nonlinearity* **1**, 409–434.

CHAIKEN, J., CHEVRAY, R., TABOR, M. & TAM, Q. M. 1986 Experimental study of Lagrangian turbulence in Stokes flow. *Proc. R. Soc. Lond.* A**408**, 165–174.

CHÁVEZ, M., ZHIXUE, W. & SEN, M. 1988 Turbulent convection in helicoidal coils. *Wärme- und Stoffübertragung* **22** (1–2), 55–60.

CHIRIKOV, B. V. 1979 A universal instability of many-dimensional oscillator systems. *Phys. Rep.* **52**, 263–379.

COX, S. M., DRAZIN, P. G., RYRIE, S. C. & SLATER, K. 1990 Chaotic advection of irrotational flows and of waves in fluids. *J. Fluid Mech.* **214**, 517–524.

ECKHARDT, B. 1990 Lagrangian chaos and transport of scalars. In *Topological Fluid Mechanics* (ed. H. K. Moffat & A. Tsinober), pp. 23–33. Cambridge University Press.

ESCANDE, D. & ELSKENS, Y. 1992 Slowly pulsating separatrices sweep homoclinic tangles where islands must be small: an extension of classical adiabatic theory. *Nonlinearity* (to appear).

GHADDAR, N. K., MAGEN, M., MIKIC, B. B. & PATERA, A. T. 1986 Numerical investigation of incompressible flow in grooved channels. part 2. Resonance and oscillatory heat transfer enhancement. *J. Fluid Mech.* **168**, 541–567.

GHOSH, S. 1991 Transport enhancement in steady and time-periodic Stokes flow between counter-rotating cylinders. MS thesis, Department of Chemical Engineering, University of Notre Dame.

GOREN, S. L. & MANI, P. V. S. 1968 Mass transfer through horizontal liquid films in wavy motion. *AIChE J.* **14**, 57–61.

GUCKENHEIMER, J. & HOLMES, P. 1983 *Non Linear Oscillations, Dynamical Systems and Bifurcations of Vector Fields.* Springer.

HOLMES, P. 1984 Some remarks on chaotic particle paths in time-periodic, three-dimensional swirling flows. *Contemp. Maths* **28**, 393–404.

KARNEY, C. F. F. 1983 Long-time correlations in the stochastic regime. *Physica* **8**D, 360–380.

MOFFAT, H. K. 1983 Transport effects associated with turbulence with particular attention to the influence of helicity. *Rep. Prog. Phys.* **46**, 621–664.

OHADI, M. M., SHARAF, N. & NELSON, D. A. 1991 Electrohydrodynamic enhancement of heat transfer in a shell-and-tube heat exchanger. *Heat Transfer* **4**, 19–39.

OTTINO, J. M. 1989 *The Kinematics of Mixing: Stretching, Chaos, and Transport.* Cambridge University Press.

RHINES, P. B. & YOUNG, W. R. 1983 How rapidly is a passive scalar mixed with closed streamlines. *J. Fluid Mech.* **133**, 133–145.

ROM-KEDAR, V. 1990 Transport rates of a class of two-dimensional maps and flows. *Physica* D**43**, 229–268.

ROM-KEDAR, V., LEONARD, A. & WIGGINS, S. 1990 An analytical study of transport, mixing and chaos in an unsteady vortical flow. *J. Fluid Mech.* **214**, 347–394.

ROSENBLUTH, M. N., BERK, H. L., DOXAS, I. & HORTON, W. 1987 Effective diffusion in laminar convective flows. *Phys. Fluids* **30**, 2636–2647.

SAGUES, F. & HORSTHEMKE, W. 1986 Diffusive transport in spatially periodic hydrodynamic flows. *Phys. Rev.* A**34**, 4136–4143.

SAXENA, A. K. & NIGAM, K. D. P. 1984 Coiled configuration for flow inversion and its effect on residence time distribution. *AIChE J.* **30**, 363–368.

SHRAIMAN, B. I. 1987 Diffusive transport in a Rayleigh–Bénard convection cell. *Phys. Rev.* A**36** (1), 261–267.

SOLOMON, T. H. & GOLLUB, J. P. 1988 Chaotic particle transport in time-dependent Rayleigh–Bénard convection. *Phys. Rev.* A**38** (12), 6280–6285.

STEWART, W. E. 1977 *Physicochemical Hydrodynamics.* V. G. Levich Festschrift. Spalding.

SWANSON, P. D. & OTTINO, J. M. 1990 A comparative computational and experimental study of chaotic mixing of viscous fluids. *J. Fluid Mech.* **213**, 227–249.

WEISS, J. B. & KNOBLOCH, E. 1989 Mass transport and mixing by modulated travelling waves. *Phys. Rev.* A**40**, 2579–2589.

YOUNG, W., PUMIR, A. & POMEAU, Y. 1989 Anomalous diffusion of tracer in convective rolls. *Phys. Fluids* A**1**, 462–469.